

# Accepted Manuscript

Discovery of 1-(3-(benzyloxy)pyridin-2-yl)-3-(2-(piperazin-1-yl)ethyl)urea: A new modulator for amyloid beta-induced mitochondrial dysfunction

Ahmed Elkamhawy, Jung-eun Park, Ahmed H.E. Hassan, Hyunhwa Ra, Ae Nim Pae, Jiyoung Lee, Beoung-Geon Park, Bongjin Moon, Hyun-Mee Park, Eun Joo Roh



PII: S0223-5234(16)31063-7

DOI: [10.1016/j.ejmech.2016.12.057](https://doi.org/10.1016/j.ejmech.2016.12.057)

Reference: EJMECH 9148

To appear in: *European Journal of Medicinal Chemistry*

Received Date: 23 August 2016

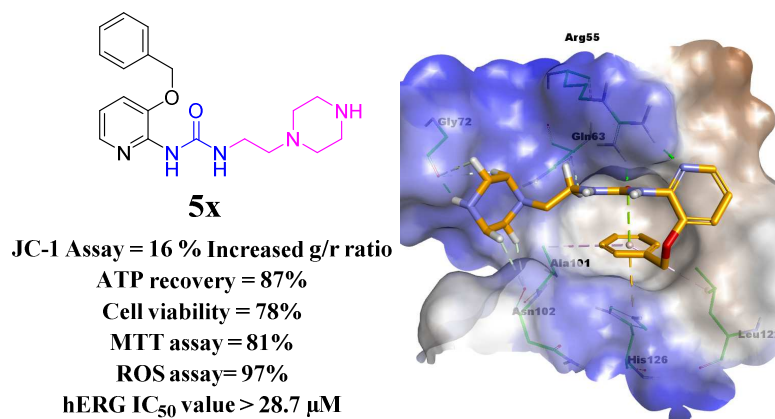
Revised Date: 15 December 2016

Accepted Date: 29 December 2016

Please cite this article as: A. Elkamhawy, J.-e. Park, A.H.E. Hassan, H. Ra, A.N. Pae, J. Lee, B.-G. Park, B. Moon, H.-M. Park, E.J. Roh, Discovery of 1-(3-(benzyloxy)pyridin-2-yl)-3-(2-(piperazin-1-yl)ethyl)urea: A new modulator for amyloid beta-induced mitochondrial dysfunction, *European Journal of Medicinal Chemistry* (2017), doi: 10.1016/j.ejmech.2016.12.057.

This is a PDF file of an unedited manuscript that has been accepted for publication. As a service to our customers we are providing this early version of the manuscript. The manuscript will undergo copyediting, typesetting, and review of the resulting proof before it is published in its final form. Please note that during the production process errors may be discovered which could affect the content, and all legal disclaimers that apply to the journal pertain.

## Graphical Abstract:



**Discovery of 1-(3-(benzyloxy)pyridin-2-yl)-3-(2-(piperazin-1-yl)ethyl)urea: a new modulator for amyloid beta-induced mitochondrial dysfunction**

**Ahmed Elkamhawy<sup>a,b,1</sup>, Jung-eun Park<sup>a,c,1</sup>, Ahmed H. E. Hassan<sup>d,e</sup>, Hyunhwa Ra<sup>a,c</sup>, Ae Nim Pae<sup>f,g</sup>, Jiyoun Lee<sup>h</sup>, Beoung-Geon Park<sup>f,i</sup>, Bongjin Moon<sup>c</sup>, Hyun-Mee Park<sup>j</sup>, Eun Joo Roh<sup>a,g,\*</sup>**

<sup>a</sup> Chemical Kinomics Research Center, Korea Institute of Science and Technology (KIST), Seoul 02792, Republic of Korea

<sup>b</sup> Department of Pharmaceutical Organic Chemistry, Faculty of Pharmacy, Mansoura University, Mansoura 35516, Egypt

<sup>c</sup> Department of Chemistry, Sogang University, Seoul 04107, Republic of Korea

<sup>d</sup> Department of Medicinal Chemistry, Faculty of Pharmacy, Mansoura University, Mansoura 35516, Egypt

<sup>e</sup> Medicinal Chemistry Laboratory, Department of Pharmacy, College of Pharmacy, Kyung Hee University, Seoul 02447, Republic of Korea

<sup>f</sup> Convergence Research Center for Diagnosis, Treatment and Care System of Dementia, Korea Institute of Science and Technology (KIST), Seoul 02792, Republic of Korea

<sup>g</sup> Department of Biological chemistry, Korea University of Science and Technology (UST), Daejeon 305-350, Republic of Korea

<sup>h</sup> Department of Global Medical Science, Sungshin Women's University, Seoul 142-732, Republic of Korea

<sup>i</sup> School of Life Sciences and Biotechnology, Korea University, Seoul 02792, Republic of Korea

<sup>j</sup> Advanced Analysis Center, Korea Institute of Science and Technology, Seoul 02792, Republic of Korea

**\*Corresponding authors: Eun Joo Roh (e-mail: [r8636@kist.re.kr](mailto:r8636@kist.re.kr)).**

<sup>1</sup> Both authors contributed equally to this work

**Abstract**

Herein, we report a new series of aliphatic substituted pyridyl-urea small molecules synthesized as potential modulators for amyloid beta ( $A\beta$ ) induced mitochondrial dysfunction. Their blocking activities against  $A\beta$ -induced mitochondrial permeability transition pore (mPTP) opening were evaluated by JC-1 assay which measures the change of mitochondrial membrane potential ( $\Delta\Psi_m$ ). The inhibitory activity of sixteen compounds against  $A\beta$ -induced mPTP opening was superior or almost similar to that of the standard Cyclosporin A (CsA). Among them, 1-(3-(benzyloxy)pyridin-2-yl)-3-(2-(piperazin-1-yl)ethyl)urea (**5x**) effectively maintained mitochondrial function and cell viabilities on ATP assay, MTT assay, and ROS assay. Using CDocker algorithm, a molecular docking model presented a plausible binding mode for **5x** with cyclophilin D (CypD) receptor as a major component of mPTP. Moreover, hERG and BBB-PAMPA assays presented safe cardiotoxicity and high CNS bioavailability profiles for **5x**. Taken as a whole, this report presents compound **5x** as a new nonpeptidyl mPTP blocker may hold a promise for further development of Alzheimer's disease (AD) therapeutics.

**Keywords:** Mitochondrial permeability transition pore (mPTP), Alzheimer's disease (AD),  $\beta$ -amyloid peptide ( $A\beta$ ), pyridyl-urea, molecular docking.

## 1. Introduction

Neurodegenerative diseases, including Alzheimer's disease, Parkinson's disease, amyotrophic lateral sclerosis and Huntington's disease, are a group of neurological disorders characterized by chronic, progressive and irreversible neuronal loss [1]. As world's population grows older because of global increase in the life expectancy, the incidence of neurodegenerative diseases is anticipated to increase consequently [2, 3]. This fact has been reflected in Alzheimer's association report estimating the number of Alzheimer's patients aged 65 or more in the US only, to almost triple, from 5.1 million in 2015, to a 13.8 million by 2050, with a rate of one new case every 33 seconds [4].

While the number of population afflicted with neurodegenerative disorders increases, effective treatments are still lacking. However, over the past two decades, better understanding of the molecular mechanisms underlying neurodegeneration offered opportunities to address new approaches for developing novel therapeutic agents combating these diseases [1, 5-8]. Mitochondrial dysfunction has been found to be a major contributor in the pathogenesis and prognosis of neurodegeneration [8-16]. Prolonged opening of mitochondrial permeability transition pore (mPTP) results in depolarization of mitochondrial membrane potential, loss of homeostasis and  $\text{NAD}^+$ , mitochondrial swelling and rupture of the outer mitochondrial membrane and finally release of apoptotic factors and cell death [17-20].

Cyclophilin D (CypD) is a mitochondrial matrix peptidyl prolyl *cis-trans* isomerase (PPI). CypD-sensitive mPTP has been found in viable human brain mitochondria [21]. The role of CypD in induction of mPTP opening leading to cell death has been validated using CypD

knockout mice [22]. Also, Amyloid  $\beta$  ( $A\beta$ ) forms a complex with CypD which enhances mPTP formation [23]. In addition, increased CypD levels has been found in Alzheimer's affected neurons [24]. Furthermore, recent studies proved the protective effect of CypD inhibitors against neurodegeneration [25]. To the best of our knowledge, up-to-date, the immunosuppressant cyclic peptide cyclosporin A (CsA) is the most significant mPTP blocker [24]. Its action is mediated *via* inhibition of CypD. Unfortunately, because of its immunosuppressant activity, as well as, its poor bioavailability and low penetration through blood brain barrier (BBB), it is used only as a probe in research [26]. Research resulted in cyclosporin A analogs devoid of immunosuppressant activity such as NIM811 and UNIL025 [27, 28]. Despite this improvement, these analogs are still far from clinical significance because of side effects and inefficiency in crossing BBB. On the other hand, few non-peptidic small molecules have been reported as mPTP inhibitors. Among seven quinoxaline derivatives, compound **1** (Figure 1) was the best selective inhibitor for CypD over CypA with micromolar activity [29]. However, to the best of our knowledge, there are no reported further efforts to develop more potent or selective derivatives belonging to this class of quinoxaline derivatives for modulation of mPTP. A series of compounds **2** (Figure 1), having 5-(halophenyl)furan-2-yl and substituted hydantoin scaffolds linked through amide spacer have been bond were found to inhibit calcium induced mitochondrial swelling, albeit with at high micromolar concentration and low potency [30]. The lack of therapeutically effective small molecule mPTP blockers stimulated our institute to launch a discovery project towards identification of promising compounds. In this project, oxime ethers **3** (Figure 1) were developed based on an oxime ether hit compound retrieved from screening of our institute chemical library [31]. This class of compounds elicited reasonable inhibition of  $A\beta$ -induced mPTP opening using JC-1 assay. Assessment of their impact on cytochrome P450 (CYP) enzymatic activities revealed

severe deterioration in CYP activity, which would leads to risks and complication of drug-drug interactions and side effects. Also in this project, a series of compounds **4** containing 1,2,3-triazole spacer as a surrogate to oxime ether were identified [32]. In comparison to oxime ether spacer in compounds **3**, the triazole spacer seems to have a function in enhancing mPTP blocking activity. In fact, 1,2,3-triazoles linkers are known as active linkers that might accept hydrogen bonds, as well as, participate in dipole-dipole and pi-stacking interactions [33].

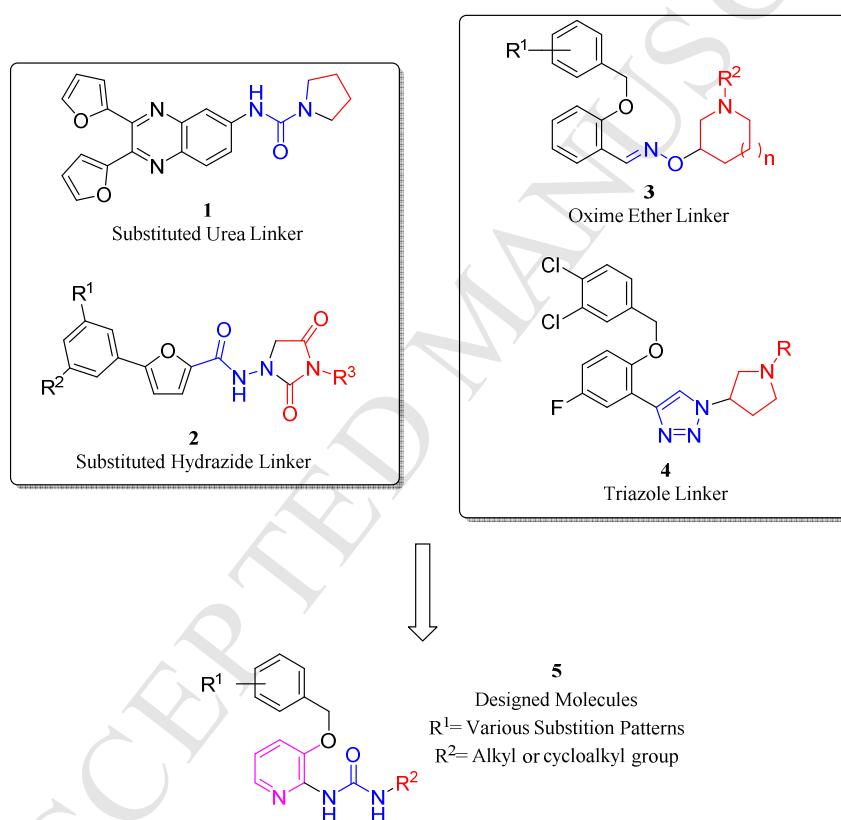


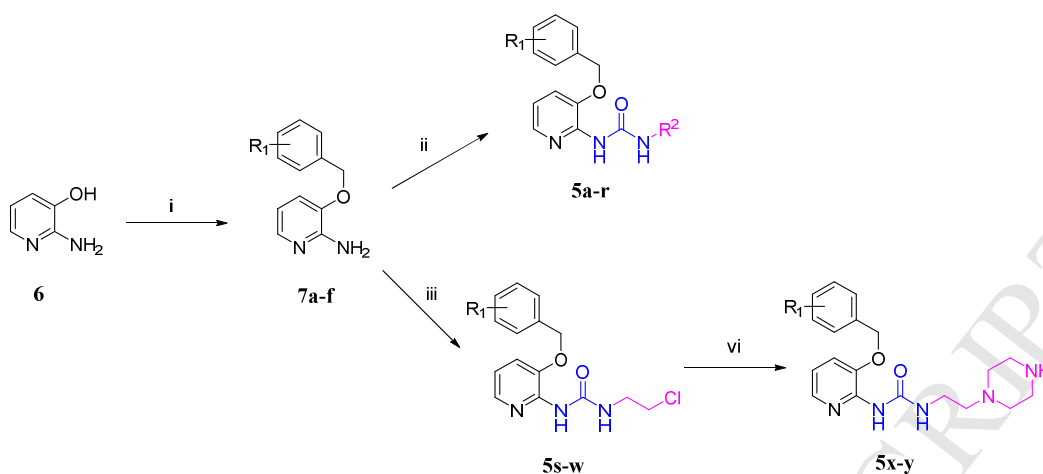
**Figure 1.** Proposed design of *N*-alkyl-*N*-2-(3-benzyloxy)pyridyl)urea derivatives *via* replacing the linker, modifying the aliphatic moiety and incorporating heterocyclic pyridine ring in the aromatic moiety.

As outlined in Figure 1, both of oxime ether in compound **3** and 1,2,3-triazole in compound **4** link 2-benzyloxyphenyl aromatic moieties, with aliphatic 3-(*N*-substituted-piperidinyl) or 3-(*N*-substituted-pyrrolidinyl) moieties, respectively. Quinoxaline compound (**1**) and furyl derivatives (**2**) have also aromatic moieties linked with aliphatic moieties through urea and hydrazide linkers respectively. As previously mentioned, the linker might have effect in enhancing the mPTP activity. Also, it can be realized that both linkers in compound **1** and furyl derivatives **2** contain hydrogen donor and acceptor groups while the 1,2,3-triazole linker in compound **4** is lacking hydrogen bond donation. In addition, the reported crystal structure of CsA-CypD complex (pdb ID = 2Z6W) reveals hydrogen bonding interactions between amide groups of CsA and Arg55, Asn102, Trp121 and His126. Accordingly, we envisioned that installing a three atoms urea linker might maintain the three atoms linker's length and may participate in binding *via* hydrogen bonding interactions. Also in our design, we switched from substituted aliphatic cyclic amines moieties to different simple alkyl or cycloalkyl groups to investigate the impact of simple aliphatic moiety on activity. In addition, the phenyl ring was modified to assess the isosteric heterocyclic pyridine ring for mPTP inhibition activity.

## 2. Results and discussion

### 2.1. Chemistry

The target pyridyl-urea derivatives were prepared according to the sequence of reactions depicted in Scheme 1. Commercially available starting material 2-amino-3-hydroxypyridine (**6**) was subjected to the S<sub>N</sub>2 displacement with various benzyl bromides under basic conditions to give 3-(benzyloxy)pyridin-2-amine derivatives (**7a–f**) which upon addition to various aliphatic isocyanates afforded compounds **5a–r** and **5s–w**. 2-Chloroethyl ureas (**5s** and **5w**) have been used as intermediates to prepare the piperazinylethyl ureas (**5x** and **5y**).



**Scheme 1.** Reagents and conditions: (i) 1) NaOH, H<sub>2</sub>O, Bu<sub>4</sub>NBr, DCM, rt, 15 min, 2) appropriate benzylbromide, DCM, rt, 18 h; (ii) appropriate isocyanate derivative, NaH (60% in mineral oil), THF, reflux, 5–18 h; (iii) 2-chloroethyl isocyanate, DIPEA, THF, reflux, 18 h; (iv) piperazine, K<sub>2</sub>CO<sub>3</sub>, acetonitrile, reflux, 20 h.

## 2.2. Biological evaluation

### 2.2.1. JC-1 assay (Mitochondrial membrane potential assay)

The ability of the synthesized compounds to inhibit the mitochondrial membrane potential loss has been evaluated using JC-1 assay [34, 35]. In this assay, JC-1 which is a lipophilic fluorescent cationic dye is used as indicator for mitochondrial membrane potential. If mitochondrial membrane potential is maintained or recovered, it forms red fluorescent J-aggregates. This red fluorescence is converted into green fluorescence when the mitochondrial membrane potential is lost. The ratio of green to red fluorescence allows the measurement of the percent of mitochondria whose membrane is affected by A $\beta$ -induced mPTP opening. Accordingly, the lower increased green to red ratio, the more effectiveness of the tested compound to block the A $\beta$ -induced mPTP opening. The ratio of green to red fluorescence is dependant only on mitochondria membrane potential and is not affected by other factors such as mitochondrial size or shape rendering the test highly specific. The results of the prepared compounds is summarized

in Table 1 and visualized in Figure 2. In the course of this test, the activity to block the A $\beta$ -induced mPTP opening was evaluated at a single dose concentration of 5  $\mu$ M. CsA was used as a positive standard where it exerted 46% of increased green to red ratio. As shown in Figure 2, sixteen compounds exhibited inhibitory activity superior or almost similar to that of the standard CsA. Three of these compounds showed high efficiency exhibiting increased ratio of green to red less than 20%. Among the tested compounds, four compounds exhibited weak or non significant inhibitory activity ranging from 64~94%. Finally, five compounds did not show any reduction in increased green to red ratio. In contrast, they exhibited elevation of the increased green to red ratio. It is noted that the most potent compounds in lead series **3** and **4** elicited 41% and 13% respectively.

Further investigation of the JC-1 assay outcome revealed mixed results. For example, while unsubstituted benzyloxy derivative **5b** bearing *tert*-butyl as the aliphatic moiety elicited potent activity with increased green to red ratio of 23%, the unsubstituted benzyloxy derivative **5a** bearing cycloheptyl moiety did not show any inhibitory activity. In contrast, the 3-chlorobenzyloxy derivative **5l** bearing *tert*-butyl as the aliphatic moiety did not show any reduction in increased green to red ratio, while the cycloheptyl derivative **5j** bearing the same 3-chlorobenzyloxy moiety elicited activity comparable to that of CsA. In the same event, all of the cycloheptyl derivatives (**5m** and **5j**) and *tert*-butyl derivatives (**5o** and **5r**) bearing 4-chlorobenzyloxy and 4-fluorobenzyloxy moieties respectively, showed nearly similar or superior to that of CsA. These results indicate that subtle stereoelectronic variations to have significant impact of the elicited biological activity.

**Table 1.** *In vitro* blocking activity of the new ureas against A $\beta$ -induced mPTP opening (JC-1 assay) at single dose concentration of 5  $\mu$ M.

Cpd	R <sub>1</sub>	R <sub>2</sub>	Increased g/r ratio (%) <sup>a</sup>	Cpd	R <sub>1</sub>	R <sub>2</sub>	Increased g/r ratio (%) <sup>a</sup>
<b>5a</b>	H	cycloheptyl	130	<b>5n</b>	4-Cl	ethyl	94
<b>5b</b>	H	<i>tert</i> -butyl	23	<b>5o</b>	4-Cl	<i>tert</i> -butyl	35
<b>5c</b>	3-F	cycloheptyl	91	<b>5p</b>	4-F	cycloheptyl	28
<b>5d</b>	3-F	1,1,3,3-tetramethylbutyl	31	<b>5q</b>	4-F	ethyl	127
<b>5e</b>	3-F	ethyl	14	<b>5r</b>	4-F	<i>tert</i> -butyl	49
<b>5f</b>	3-F	<i>tert</i> -butyl	44	<b>5s</b>	H	–	169
<b>5g</b>	2-Cl	cycloheptyl	41	<b>5t</b>	3-Cl	–	73
<b>5h</b>	2-Cl	1,1,3,3-tetramethylbutyl	21	<b>5u</b>	2-Cl	–	41
<b>5i</b>	2-Cl	ethyl	49	<b>5v</b>	4-Cl	–	131
<b>5j</b>	3-Cl	cycloheptyl	46	<b>5w</b>	4-F	–	64
<b>5k</b>	3-Cl	1,1,3,3-tetramethylbutyl	50	<b>5x</b>	H	–	16
<b>5l</b>	3-Cl	<i>tert</i> -butyl	176	<b>5y</b>	3-Cl	–	48
<b>5m</b>	4-Cl	cycloheptyl	19	CsA	–	–	46

<sup>a</sup> % Increase of fluorescence-ratio (green/red) after treatment of each compound and A $\beta$  with regard to that of A $\beta$  alone (100%). See the text for more detailed information.

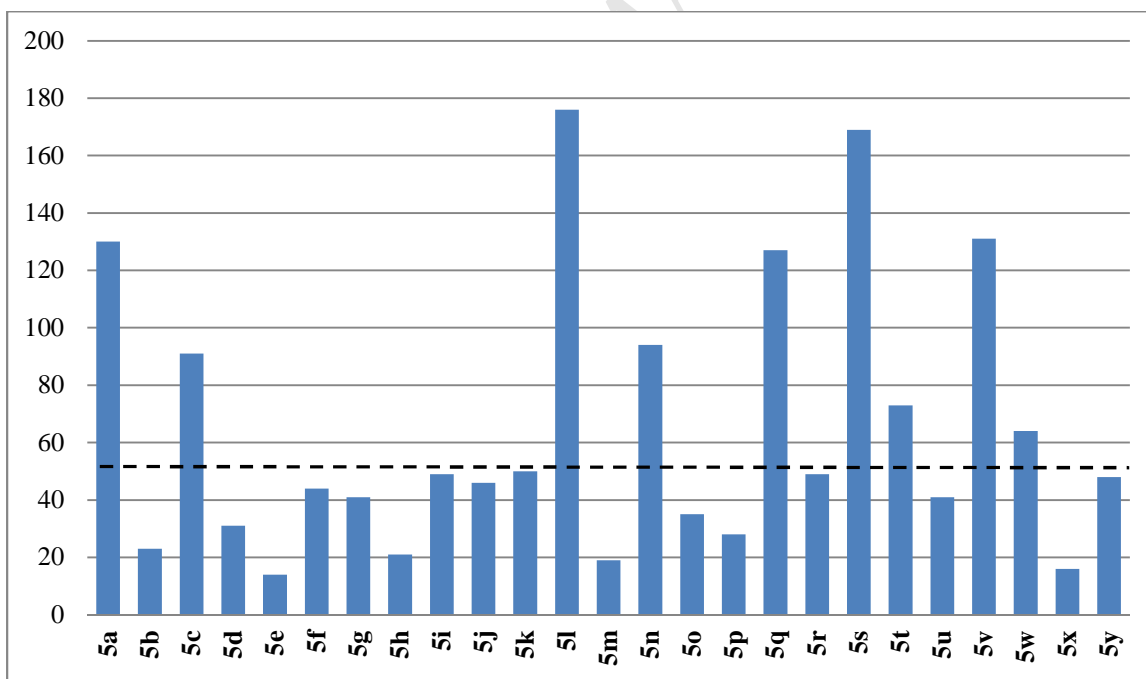


**Figure 2.** Percentage increase in the fluorescence ratio (green/red) after treatment of each compound and A $\beta$  with respect to that of A $\beta$  alone (100%). Y-axis represents the percent of increased green to red fluorescence ratio of each compound. Dashed line represents the percent of increased green to red fluorescence ratio of Cyclosporin A (CsA) used as a control.

### 2.2.2. ROS production and MTT cell viability assay

In drug discovery processes, it is beneficial to perform a front *in vitro* testing of toxicities. This would enable early detection and exclusion of potential toxic molecules; thus reducing the number of unfavorable compounds and focusing efforts on the more likely safe candidates. Accordingly, the intrinsic ability of a set of the most active compounds in JC-1 assay to induce production of reactive oxygen species (ROS) and cytotoxicity was assessed in neuro-2a cells using 10-dose 3-fold serial dilutions. As Table 2 shows, all tested compounds did not show significant increase of hydrogen peroxide levels up to a dose of 10  $\mu\text{M}$  concentration which is double the dose used in JC-1 assay. In comparison, at 10  $\mu\text{M}$  concentration, the standard menadione elicited approximately seven times-elevation of hydrogen peroxide level with  $\text{IC}_{50} = 2.688 \mu\text{M}$ . This indicates that these compounds can't induce ROS formation which is an important consideration in assessment of toxicity. In addition, almost all tested compounds exhibited excellent cell viability in cytotoxicity tests using MTT assay with doses up to 10  $\mu\text{M}$  concentration. At this dose, the standard staurosporine elicited only 1.3% viability with  $\text{IC}_{50} = 0.0113 \mu\text{M}$ .

**Table 2.** Results of induction of ROS production and cytotoxicity up to 10  $\mu\text{M}$  concentrations

Cpd	ROS		MTT viability <sup>c</sup>		Cpd	ROS		MTT viability	
	Fold of H <sub>2</sub> O <sub>2</sub> Production <sup>a</sup>	IC <sub>50</sub> <sup>b</sup>	% Viability <sup>c</sup>	IC <sub>50</sub> <sup>b</sup>		Fold of H <sub>2</sub> O <sub>2</sub> Production <sup>a</sup>	IC <sub>50</sub> <sup>b</sup>	% Viability <sup>c</sup>	IC <sub>50</sub> <sup>b</sup>
<b>5b</b>	0.92	> 10	106.1	> 10	<b>5o</b>	0.91	> 10	93.1	> 10
<b>5d</b>	1.02	> 10	101.4	> 10	<b>6p</b>	0.91	> 10	93.2	> 10
<b>5e</b>	1.14	> 10	96.6	> 10	<b>5x</b>	0.97	> 10	101.8	> 10
<b>5f</b>	0.94	> 10	95.8	> 10	<b>Menadione</b>	6.94	2.688		
<b>5m</b>	1.15	> 10	85.25	> 10	<b>Staurosporine</b>			1.3	0.0116

<sup>a</sup> Folds of produced H<sub>2</sub>O<sub>2</sub> by neuro-2a cells after 6 hours incubation with 10  $\mu\text{M}$  concentration of each compound relative to non-treated.

<sup>b</sup> IC<sub>50</sub> expressed in  $\mu\text{M}$  concentration.

<sup>c</sup> % Viability of neuro-2a cells after 72 hours incubation with 10  $\mu\text{M}$  concentration of each compound.

### 2.2.3. Assay for cellular ATP levels (Luciferase-based assay)

To identify likely-safe and promising compounds for further testing and development, the next filter in the adopted discovery workflow was rationalized on that promising compounds should not impair ATP production, and preferably, protect neurons against A $\beta$ -induced impairment of ATP production. This is because a main role for the mitochondria is the production of ATP. Candidates able to block detrimental A $\beta$ -induced mPTP opening should eventually repair mitochondrial dysfunction by promoting ATP generation. A luciferase-based assay for cellular ATP levels was carried out to validate the effect of selected set of the most active compounds on mitochondrial function [36]. As shown in Table 3, among the tested compounds, compounds **5b** and **5x**, bearing unsubstituted benzyloxy group, possessed highest inhibitory activity against A $\beta$ -induced ATP reduction as well as reasonable cell viability, which are comparable to those of piracetam. Thus, compounds **5b** and **5x** were advanced to further investigations.

**Table 3.** The result of ATP assay of the tested compounds

Cpd	ATP Viability <sup>a</sup>	% Recovery <sup>b</sup>	Cpd	ATP Viability <sup>a</sup>	% Recovery <sup>b</sup>
<b>5b</b>	<b>103</b>	<b>72</b>	<b>5o</b>	104	13
<b>5d</b>	30	-140	<b>6p</b>	99	40
<b>5e</b>	102	41	<b>5x</b>	<b>78</b>	<b>87</b>
<b>5f</b>	129	45	<b>Piracetam</b>	88	127
<b>5m</b>	105	47			

<sup>a</sup> % Viability of hippocampal neuronal cell line HT-22 was calculated based on ATP production after 7 hours incubation with 5  $\mu$ M of each compound.

<sup>b</sup> % Recovery of ATP production by A $\beta$ -suppressed mitochondrial ATP production in hippocampal neuronal cell line HT-22 after 7 hours incubation with 5  $\mu$ M of each compound.

### 2.2.4. Protection against A $\beta$ -induced ROS production and cytotoxicity

A $\beta$  induces cytotoxicity *via* multiple mechanisms, and furthermore, the exact A $\beta$  toxic polymorph and species are still controversial [37-42]. Despite these controversies about the mechanisms of A $\beta$ -induced cytotoxicity, protection against A $\beta$ -induced cytotoxicity is a

desirable feature for development of an effective Alzheimer's disease therapy. Accordingly, assays of the overall protective activity of prepared compounds against A $\beta$ -induced cytotoxicity were incorporated in the adopted workflow. Next to JC-1 assay, compound's triggered ROS production and cytotoxicity assay, and the luciferase-based ATP assay; subsequent filters were applied to test the capability of compounds for protection of hippocampal neuronal cells against A $\beta$  induced ROS production and cytotoxicity. In this regard, MTT assay was carried out to evaluate the mitochondrial dehydrogenase activity as well as a CM-H<sub>2</sub>DCFDA-fluorescent assay to measure the cellular reactive oxygen species (ROS) resulting from A $\beta$  toxicity [43, 44]. As listed in Table 4, compound **5x** reduced A $\beta$ -induced toxicity in the MTT assay with 81% compared to 29% of the standard piracetam. It also reduced A $\beta$ -induced ROS production with 97% inhibition value. These data suggested that compound **5x** as a potential mPTP blocker maintaining mitochondrial function and cell viability.

**Table 4.** Results of MTT assay, ROS assay and BBB diffusion assay of **5b** and **5x**

Compound	% Inhibition of A $\beta$ -induced ROS <sup>a</sup>	% Viability <sup>b</sup>	% Inhibition of A $\beta$ -induced cytotoxicity <sup>c</sup>	Effective Permeability <sup>d</sup> P <sub>e</sub> (10 <sup>-6</sup> cm/sec)
<b>5b</b>	95	92	11	45.14
<b>5x</b>	97	133	81	20.63
Piracetam	129	132	29	
Progesterone				48.81
Lidocaine				26.56
Theophylline				0.29

<sup>a</sup> Percent inhibition of A $\beta$ -induced ROS production by A $\beta$ -treated hippocampal cell line HT-22 after 6 hours incubation with 5  $\mu$ M of each compound.

<sup>b</sup> % Viability of hippocampal cell line HT-22 after 24 hours incubation with at 5  $\mu$ M of each compound.

<sup>c</sup> % Viability of A $\beta$ -suppressed hippocampal cell line HT-22 after 24 hours incubation with at 5  $\mu$ M of each compound.

<sup>d</sup> Effective permeability (P<sub>e</sub>) was measured at 50  $\mu$ M concentrations after 4 hours of passive diffusion using Pion PAMPA-BBB.

### 2.2.5. Parallel artificial membrane permeability assay (artificial BBB diffusion assay)

Molecules to be developed for treatment of CNS disorders must be able to overcome the natural obstacle of blood brain barrier (BBB) to reach their actions targets within CNS. Without appropriate capacity to penetrate BBB, *in vitro* active candidates would be useless *in vivo*. Therefore, compounds **5b** and **5x** were submitted for evaluation of their tendency to cross blood-brain barrier using parallel artificial membrane permeability assay (PAMPA) [45, 46]. Three standard drugs were used for calibration and comparison. The following effective permeability ( $P_e$ ) ranges were established in this assay: no penetration of BBB ( $P_e < 0.4 \times 10^{-6}$  cm/sec), penetration of BBB ( $P_e > 0.4 \times 10^{-6}$  cm/sec), low CNS bioavailability ( $P_e < 10 \times 10^{-6}$  cm/sec), and high CNS bioavailability ( $P_e > 10 \times 10^{-6}$  cm/sec). As shown in Table 4, theophylline which poorly diffuse across BBB, had measured effective permeability  $P_e = 0.29 \times 10^{-6}$  cm/sec, while lidocaine and progesterone which highly cross BBB had effective permeability of  $P_e = 26.56 \times 10^{-6}$  and  $48.81 \times 10^{-6}$  cm/sec respectively. In comparison, compounds **5X** and **5b** had measured effective permeability  $P_e = 20.63 \times 10^{-6}$  and  $45.14 \times 10^{-6}$  cm/sec respectively indicating their high CNS bioavailability.

#### 2.2.6. Molecular Modeling Study

As mentioned before, CypD is a mitochondrial peptidyl prolyl *cis-trans* isomerase PPI that plays an important role in mPTP opening and loss of membrane potential [22]. The cyclic polypeptide CsA effectively binds and inhibits CypD. Investigation of the reported crystal of human CypD-CsA complex (pdb ID = 2Z6W) reveals hydrophobic interactions as the major contributor in binding [47]. CypD residues interacting with bound CsA can be differentiated into distinctive regions. First, there is a hydrophobic pocket 1 formed by residues Met61, Ala101, Phe113, Leu122 and His126. In this pocket, the CsA's methylated valine residue (Mva11) elegantly fits.

A saddle formed of Gln63 and Asn102, separates pocket 1 from another less hydrophobic pocket 2 in which the CsA's  $\alpha$ -amino-butyric acid residue (Aba2) is interacting with Gln111 and Gly72. On the other side next to pocket 1, there is a flattened hydrophobic surface formed of Phe60, Ile57 and Trp121, with which the side chain of CsA's methylated leucine residue (Mle9) is interacting. In addition, side chain of the 4-(2-butenyl)-4-methylthreonine residue (Bmt1) shows hydrophobic interaction with a nearby Ala103 residue. Hydrogen bonding interactions are observed mainly with amino acids Gln63 and Asn102 in the saddle region, Arg55 and His126 at the edge of pocket 1, and Trp121 in the flattened hydrophobic surface next to pocket 1.

In order to understand the outcome of mitochondrial membrane potential assay, molecular modeling study was conducted to get insights into the molecular factors that might underlie the observed biological activity. A set of most effective mPTP blockers (**5b**, **5d**, **5e**, **5h**, **5m**, **5o**, **5p**, and **5x**) and another set of ineffective mPTP blockers (**5a**, **5c**, **5l**, **5n**, **5q**, **5s** and **5v**) were docked into the reported crystal structure of human CypD (pdb ID = 2Z6W) after appropriate preparation of receptor and ligands. The CHARMM force field based docking CDocker algorithm implemented in Accelrys Discovery Studio 4.0 was used as a flexible docking method to predict the binding mode of different ligands to CypD [48]. This algorithm is characterized by employing explicit all-atoms CHARMM force field calculations which outperforms algorithms based on grid-based approximations in accurate prediction of correct pose. The resulting poses were further refined by *in situ* minimizations and the binding energies and complexes energies were calculated. Selection of the most probable binding modes was based on these calculated energy terms.

The predicted binding modes for this series of compounds can be generally grouped under two broad binding modes. The first one, which is more preferable by active ligands, is characterized by part of ligand being bound within the hydrophobic pocket 1 eliciting interactions with the residues forming this pocket. On the other hand, the second mode, which is more prevalent in inactive ligands, shows no binding within this hydrophobic pocket 1. Instead, the docked ligand tends to flip out of binding pocket 1 exhibiting bind above the pocket.

The different binding modes for the most effective mPTP blocker **5e** are illustrated in Figure 3. Out of twenty retrieved different poses, compound **5e** elicited nineteen poses belonging to general mode 1 and only one pose belonging to general mode 2. The energy terms for binding mode 1 in the best calculated pose were estimated to be -52.55 kcal/mol for binding energy, -49.77 kcal/mol for total binding energy and -2933.91 kcal/mol for complex energy. In comparison, the energy terms for only one detected pose belonging to general binding mode 2 were -44.99 kcal/mol for binding energy, -38.22 kcal/mol for total binding energy and -2929.09 kcal/mol for complex energy. Total binding poses belonging to mode 1, which were superior to binding mode 2, are eight poses in terms of binding energy, nine poses in terms of total binding energy and eight poses with in terms of complex stability. This indicates a high tendency of compound **5e** to bind in mode 1 rather than mode 2.

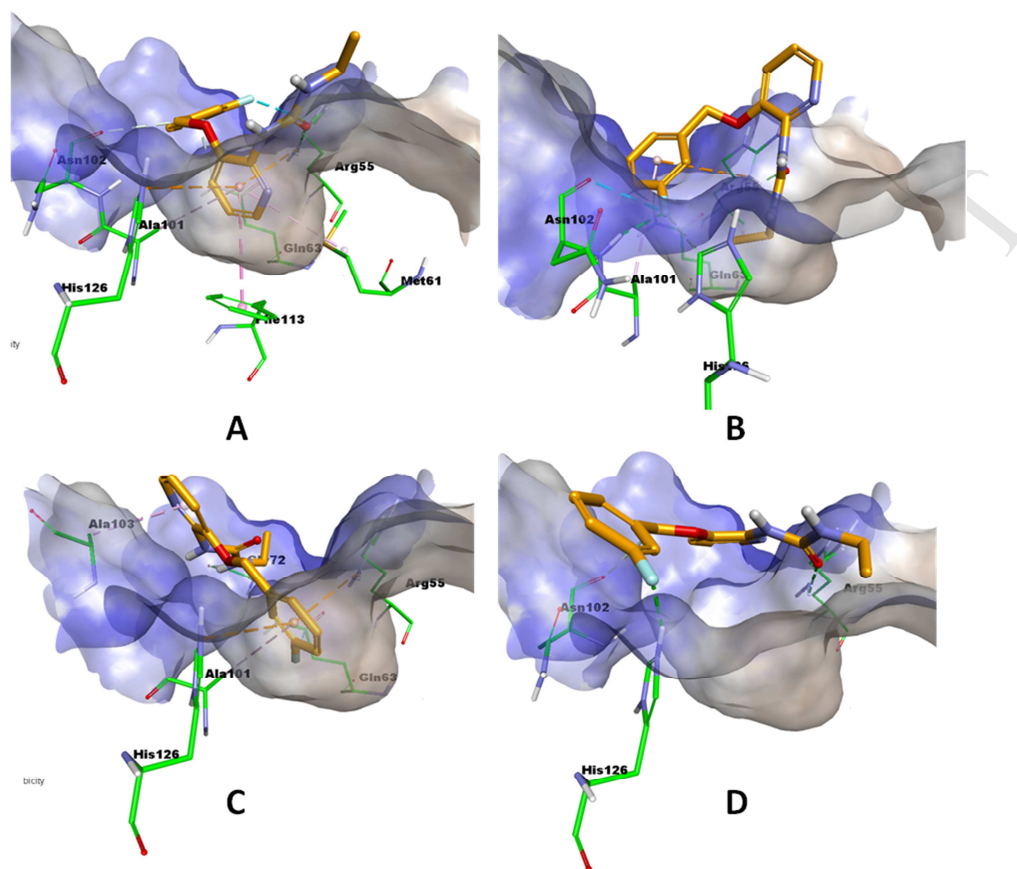


**Figure 3.** Different Binding modes of compound **5e**; A) Binding mode 1 subtype 1; in which the pyridine ring docks into the hydrophobic pocket 1. B) Binding mode 1 subtype 2; in which the aliphatic moiety docks into the hydrophobic pocket 1. C) Binding mode 1 subtype 3; in which the aromatic ring of the benzyloxy moiety docks into the hydrophobic pocket 1. D) Binding mode 2; in which the hydrophobic pocket 1 is vacant while compound **5e** is docked above it.

Within the general binding mode 1, three different sub-modes were identified. As shown in Figure 3A, in binding mode 1 subtype 1, the aromatic pyridine ring docks into the hydrophobic pocket 1. This subtype of mode 1 was detected in seven out of the eight poses having energy terms superior to binding mode 2. The best pose in terms of energy belongs to this subtype of binding mode. In this pose, the pyridine ring is involved in interactions with residues of pocket 1 forming pi-pi T-shaped interaction with Phe113, pi-alkyl interaction with Ala101 and Met61 and pi-cation interaction with Arg55 and His126. The urea linker is involved in hydrogen bonding

interactions with Arg55. The aliphatic ethyl moiety is directed towards the hydrophobic surface adjacent to pocket 1. The benzyloxy moiety is involved in two non-classical hydrogen bonding interactions between Asn102 and Gln63 in the saddle region with benzylic hydrogen and the aromatic ring respectively. Fluorine substitution on the benzyloxy ring is involved in halogen interaction with side chain of Arg55. It should be noted that poses belonging to this subtype shared the criteria of pyridine ring docked into the pocket, albeit, it was rotated within the pocket resulting in different orientations of benzyloxy and aliphatic urea groups.

In subtype 2 of binding mode 1 (Figure 3B), which has been detected in five poses, the aliphatic moiety is docked into the hydrophobic pocket 1. Despite the calculated energy terms of the best scoring pose in binding mode 1 subtype 2 (-45.52 kcal/mol for binding energy, -43.30 kcal/mol for total binding energy and -2931.64 kcal/mol for complex energy) are much less favorable than that for the best performing pose in binding mode 1 subtype 1, it is still energetically more favorable than mode 2, especially in terms of total binding energy and complex energy. Although the docked aliphatic ethyl moiety into the hydrophobic pocket, the more pronounced interactions were benzyloxy moiety pi-cation interactions with Arg55, non classical pi-hydrogen bond with Gln63, pi-alkyl interaction with Ala101, halogen-hydrogen bond with NH of Asn102, halogen-acceptor interaction with CO of Asn102, and Hydrogen bond with His126. The urea linker was involved in hydrogen bonding interaction with Arg55.

In subtype 3 of binding mode 1 (Figure 3C), which has been detected only in one pose, the benzyloxy moiety is docked into the hydrophobic pocket 1. The most pronounced interactions in this mode are two pi-cation interactions between benzyloxy ring with Arg55 and His126, pi-alkyl

interaction of benzyloxy ring with Ala101, halogen acceptor interaction of fluorine atom on benzyloxy ring with Gln63, pi-alkyl interaction of pyridine ring with Ala103, and hydrogen bond of urea with Gly72. The calculated energy terms (-31.08 kcal/mol for binding energy, -27.97 kcal/mol for total binding energy and -2917.78 kcal/mol for complex energy) indicate that mode 1 subtype 3 is energetically much less favored than all of mode 2 and other mode 1 subtypes.

Binding mode 2 is illustrated in Figure 3D. This mode, which has been detected only in one pose, is characterized by unoccupied hydrophobic pocket 1. The ligand in this mode docks above the pocket. The most pronounced interactions in this mode are hydrogen bonds between urea with Arg55, benzylic hydrogens with Asn102, and halogen-hydrogen bond between the fluorine with His126. Considering all of previously mentioned binding modes in conjunction with their calculated energy terms, the potent activity of compound **5e** can be attributed to dominating binding mode 1 subtype 1.

Similar analysis of calculated binding modes of the active and inactive sets revealed the anticipated binding modes behind the biological performance of tested compounds for blocking mPTP. For example, the high efficiency of compound **5x** to block mPTP was attributed to a variant of binding mode 1 subtype 3 (Figure 4A), where the benzyloxy group is docked into the hydrophobic pocket 1. In this variant, the pyridyl ring is facing the hydrophobic surface adjacent to the hydrophobic pocket 1, and the urea linker along with the ethyl chain are extended to direct the piperazine ring towards the less hydrophobic pocket which in turn shows interactions non-classical and classical hydrogen bonding interactions between Gly72 in the pocket and Asn102 in the saddle with piperazine ring. Other pronounced interactions are non-classical hydrogen

bond interactions of hydrogens in ethyl chain with Gln63 in the saddle, classical hydrogen bonding interactions between Arg55 and urea linker and pyridyl's nitrogen, pi-alkyl interactions of benzyloxy ring with both of Leu122 and Ala101, in addition to pi-cation interaction with His126. It is noted that there is pi-lone pair interaction between the benzyloxy ring and the oxygen atom in the urea linker which contributes to the stabilization of this bent conformation. The calculated energy terms (-66.38 kcal/mol for binding energy, -52.28 kcal/mol for total binding energy, and -2930.12 kcal/mol for complex energy), along with elicited binding mode, provide a good explanation for the high efficiency of this ligand in blocking mPTP.

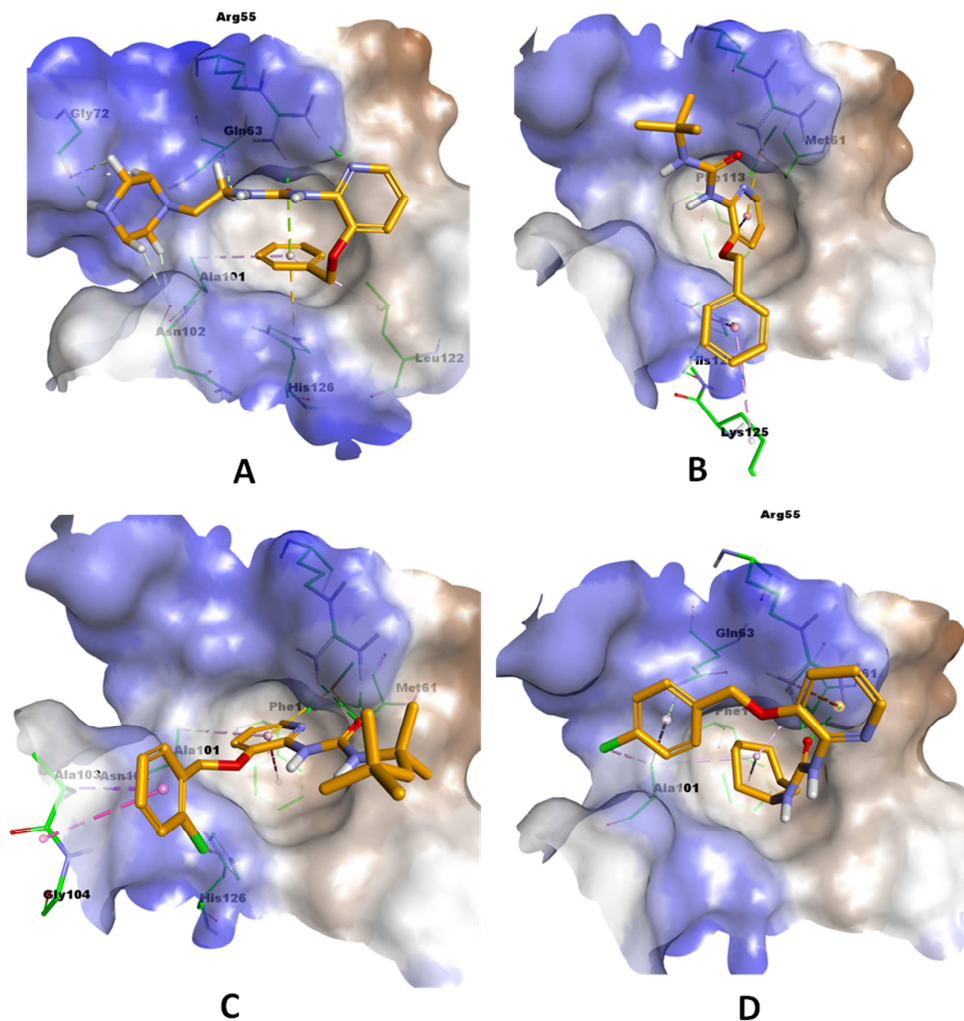


**Figure 4.** The most favorable binding modes of selected examples of active ligands. A) Compound **5x** binding mode 1 **subtype 3**, in which the benzyloxy moiety is docked into the hydrophobic pocket 1. B) Compound **5b** binding mode 1 subtype 1, in which the pyridine is docked into the hydrophobic pocket 1 with 90° rotation within the pocket. C) Compound **5h** binding mode 1 subtype 1, in which the pyridine is docked into the hydrophobic pocket 1 D) Compound **5m** binding mode 1 **subtype 2**, in which the cycloheptyl ring is docked into the hydrophobic pocket 1.

The most probable binding modes for selected examples of active compounds from the docked active set are displayed in Figure 4. As illustrated, Compounds **5b** and **5h** elicit their activities *via* different variants of binding mode 1 subtype 1. The pyridine rings of the two docked ligands show 90° rotation within the hydrophobic pocket in relation to each other. Accordingly, the aliphatic moiety and benzyloxy moiety occupy different orientations. Also, as illustrated, compound **5m** elicit activity through a variant of binding mode 1 subtype 2. In this case, the cycloheptyl ring of the ligand is docked into the hydrophobic pocket 1.

Application of this protocol of docking and analysis to the set of inefficient mPTP blockers revealed general dominance of binding mode 2. Accordingly, it can be anticipated that this mode might be responsible for their observed inefficiency as mPTP blockers. As Figure 5A illustrates, in some compounds exemplified by compound **5a**, binding mode 2 dominates exclusively. While in some compounds, exemplified by compound **5c** with very weak blocking activity (91% increased green to red in JC-1 assay), both binding mode 1 subtype 1 (Figure 5B) and mode 2 (Figure 5C) were detected in close calculated energy terms for both modes (for mode 1 subtype 1, -54.34 kcal/mol for binding energy, -50.54 kcal/mol for total binding energy and -2926.6 kcal/mol for complex energy; for mode 2, -52.23 kcal/mol for binding energy, -48.04 kcal/mol for total binding energy and -2925.59 kcal/mol for complex energy).

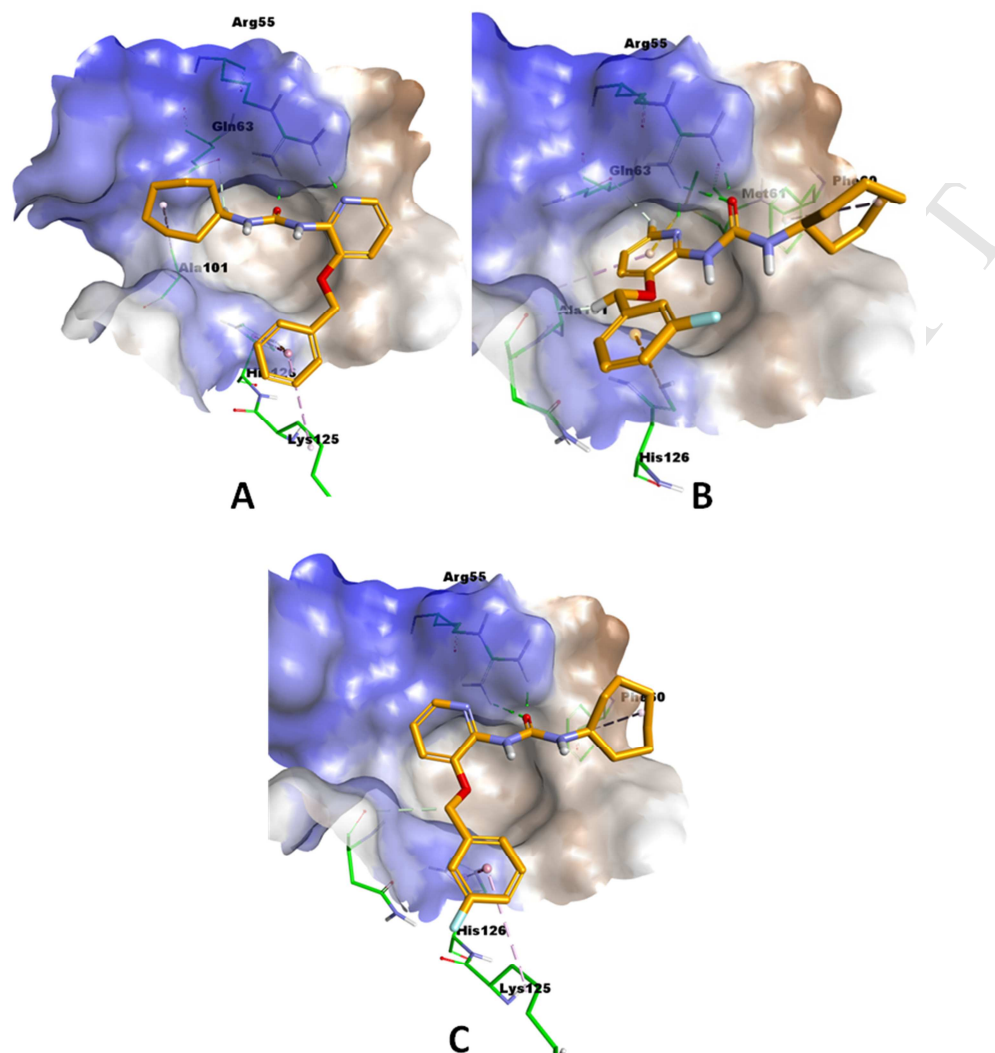


**Figure 5.** The most favorable binding modes of selected inefficient mPTP blocker; A) Compound **5a** binding mode 2, in which no binding within the hydrophobic pocket is observed. B) Compound **5c** binding mode 1 subtype 1, in which pyridine ring is docked into the hydrophobic pocket. C) Compound **5c** binding mode 2, in which the hydrophobic pocket is vacant.

The current modeling study revealed clearly distinguishable binding modes that can provide an explanation for the observed activity of the tested series of 3-((benzyloxy) pyridin-2-yl) aliphatic urea derivatives.

### 2.2.7. hERG K<sup>+</sup> channel binding affinity (Cardiotoxicity measurement)

Recently some small molecules were withdrawn from the market because they induced the prolongation of the QT interval of the surface electrocardiogram (ECG) by blocking the human ether-a-go-go related gene (hERG) potassium channel. Blockade of the hERG channel is a significant hurdle in lead optimization activity due to its potential cardiotoxicity [49, 50]. Thus, we measured the hERG affinity of compound **5x**. The test demonstrated an excellent result ( $IC_{50}$  value  $> 28.7 \mu\text{M}$ ), which means that the compound under test doesn't have blockage activity towards the hERG channel and then it is considered as safe compound with regard to the potential cardiotoxicity.

### 3. Conclusion

In this study, compound **5x** has been discovered as a new mPTP modulator efficiently protecting mitochondria against  $A\beta$  induced mitochondrial membrane depolarization. It elicited good *in vitro* profile with regard to the assays associated with mitochondrial functions and cell viabilities. Moreover, the *in silico* study provided rational explanation of the observed activity. *In vitro* cardiotoxicity test of **5x** showed promising results. Therefore, compound **5x**, a potential mPTP blocker, may serve as a good lead for further development of new AD therapeutics.

## 4. Experimental

### 4.1. Chemistry

General: All reactions and manipulations were performed in nitrogen atmosphere using standard Schlenk techniques. The reaction solvents purchased from Aldrich Co., TCI and Alfa and used without any other purification. The NMR spectra were obtained on Bruker Avance 300 or 400.  $^1\text{H}$  NMR spectra were referenced to tetramethylsilane ( $\delta = 0.00$  ppm) as an internal standard and

are reported as follows: chemical shift, multiplicity (br = broad, s = singlet, d = doublet, t = triplet, dd = doublet of doublet, m = multiplet).  $^{13}\text{C}$  NMR spectra were referenced to the residual  $\text{CDCl}_3$  ( $\delta = 77.0$  ppm). Column chromatography was performed on Merck Silica Gel 60 (230–400 mesh) and eluting solvents for all of these chromatographic methods are noted as appropriated-mixed solvent with given volume-to-volume ratios. TLC was carried out using glass sheets pre-coated with silica gel 60 F<sub>254</sub> purchased by Merk. The purity of samples was determined by analytical HPLC using a Waters ACQUITY UPLC (CORTECS™) with C18 column (2.1 mm  $\times$  100 mm; 1.6  $\mu\text{m}$ ) at temperature 40 °C. HPLC data were recorded using parameters as follows: 0.1% formic acid in water and 0.1% formic acid in methanol, 30/70 gradient in 10 min, and flow rate of 0.3 mL/min. High-resolution spectra were performed on Waters ACQUITY UPLC BEH C18 1.7 $\mu$ -Q-TOF SYNAPT G2-Si High Definition Mass Spectrometry.

#### 4.1.1. General procedure of 3-(benzyloxy)pyridin-2-amine derivatives (7a–f)

Sodium hydroxide (6 g, 0.15 mol) was dissolved in water (10 mL) and mixed with dichloromethane (15 mL). 2-Amino-3-hydroxy pyridine (**6**, 3 g, 27.24 mmol) was added to the reaction mixture in portions, under stirring, followed by the catalyst, tetrabutylammonium bromide (156 mg, 0.48 mmol). The reaction mixture was stirred for 15 min at 25–30 °C, and treated with a solution of the appropriate benzyl bromide derivative (5.4 g, 28.61 mmol) in dichloromethane (10 mL). The reaction mixture was stirred 18 h at 25 °C and then diluted with water (15 mL). The organic phase was separated, and the aqueous phase was extracted with dichloromethane. The organic extracts were combined, washed with water and brine, dried over sodium sulfate, filtered and evaporated under reduced pressure. The residue was purified by

column chromatography (SiO<sub>2</sub>, EA/*n*-Hex = 1/2). For 3-(benzyloxy)pyridin-2-amine **7a**, it has been purchased from Alfa Aesar Co.

### **3-(3-fluorobenzyloxy)pyridin-2-amine (7b)**

Light pink solid, yield: 70%, <sup>1</sup>H NMR (400 MHz, CDCl<sub>3</sub>) δ = 4.68 (2H, brs, NH<sub>2</sub>), 5.06 (2H, s, OCH<sub>2</sub>Ph), 6.58 (1H, dd, *J* = 5.1 Hz, 7.8 Hz, ArH), 6.93 (1H, dd, *J* = 1.1 Hz, 7.8 Hz, ArH), 7.04 (1H, td, *J* = 2.4 Hz, 8.4 Hz ArH), 7.14 (1H, dd, *J* = 2.0 Hz, 9.4 Hz, ArH), 7.18 (1H, d, *J* = 7.6 Hz, ArH), 7.36 (1H, td, *J* = 5.8 Hz, 8.0 Hz, ArH), 7.69 (1H, dd, *J* = 1.3 Hz, 5.1 Hz, ArH).

### **3-(3-chlorobenzyloxy)pyridin-2-amine (7c)**

Light yellow solid, yield: 66%, <sup>1</sup>H NMR (400 MHz, DMSO-*d*<sub>6</sub>) δ = 5.13 (2H, s, OCH<sub>2</sub>Ph), 5.72 (2H, brs, NH<sub>2</sub>), 6.47 (1H, dd, *J* = 5.0 Hz, 7.7 Hz, ArH), 7.07 (1H, d, *J* = 7.8 Hz, ArH), 7.37–7.47 (3H, m, ArH), 7.51 (1H, dd, *J* = 1.2 Hz, 5.0 Hz, ArH), 7.58 (1H, s, ArH). Reported [51].

### **3-(2-chlorobenzyloxy)pyridin-2-amine (7d)**

Yellow solid, yield: 88%, <sup>1</sup>H NMR (400 MHz, CDCl<sub>3</sub>) δ = 4.73 (2H, brs, NH<sub>2</sub>), 5.18 (2H, s, OCH<sub>2</sub>Ph), 6.59 (1H, dd, *J* = 5.1 Hz, 7.8 Hz, ArH), 6.96 (1H, d, *J* = 7.8 Hz, ArH), 7.27–7.31 (2H, m, ArH), 7.40–7.43 (1H, m, ArH), 7.46–7.48 (1H, m, ArH), 7.69 (1H, d, *J* = 5.0 Hz, ArH). Reported [51].

### **3-(4-chlorobenzyloxy)pyridin-2-amine (7e)**

Yellow solid, yield: 53%,  $^1\text{H}$  NMR (400 MHz,  $\text{CDCl}_3$ )  $\delta$  = 4.66 (2H, brs,  $\text{NH}_2$ ), 5.03 (2H, s,  $\text{OCH}_2\text{Ph}$ ), 6.59 (1H, dd,  $J$  = 5.1 Hz, 7.8 Hz, ArH), 6.93 (1H, dd,  $J$  = 1.3 Hz, 7.8 Hz, ArH), 7.29–7.46 (4H, m, ArH), 7.69 (1H, dd,  $J$  = 1.3 Hz, 5.1 Hz, ArH). Reported [52].

### 3-(4-fluorobenzyloxy)pyridin-2-amine (7f)

White solid, yield: 26%,  $^1\text{H}$  NMR (400 MHz,  $\text{CDCl}_3$ )  $\delta$  = 4.64 (2H, brs,  $\text{NH}_2$ ), 5.02 (2H, s,  $\text{OCH}_2\text{Ph}$ ), 6.59 (1H, dd,  $J$  = 5.1 Hz, 7.8 Hz, ArH), 6.93 (1H, dd,  $J$  = 1.1 Hz, 7.8 Hz, ArH), 7.08 (2H, t,  $J$  = 8.7 Hz, ArH), 7.37–7.40 (2H, m, ArH), 7.68 (1H, dd,  $J$  = 1.3 Hz, 5.1 Hz, ArH). Reported [51].

#### 4.1.2. General procedure of urea compounds (5a–r)

2-amino-3-benzyloxy pyridine derivative (0.85 mmol) and sodium hydride (60% in mineral oil, 68 mg, 1.71 mmol) was dissolved in dry THF (5 mL), aliphatic isocyanate derivative (1.02 mmol) was added to the reaction mixture. The reaction was refluxed for 5–18 h. After cooling, the reaction mixture was evaporated and the residue was purified by flash column chromatography ( $\text{SiO}_2$ , EA/*n*-Hex = 1/4) to afford the title final compounds **5a–r**.

### 1-(3-(benzyloxy)pyridin-2-yl)-3-cycloheptylurea (5a)

White solid, yield: 80%, mp: 111–112 °C, HPLC purity: 3.97 min, 92.14%,  $^1\text{H}$  NMR (400 MHz,  $\text{CDCl}_3$ )  $\delta$  = 1.56–1.66 (10H, m,  $5\text{CH}_2$ ), 1.95–2.00 (2H, m,  $\text{CH}_2$ ), 4.01–4.03 (1H, m, CH), 5.09 (2H, s,  $\text{OCH}_2\text{Ph}$ ), 6.76–6.79 (1H, dd,  $J$  = 5.1 Hz, 8.0 Hz, ArH), 7.06 (1H, d,  $J$  = 8.0 Hz, ArH), 7.33 (1H, s, NH), 7.35–7.39 (5H, m, ArH), 7.76 (1H, d,  $J$  = 5.1 Hz, ArH), 9.53 (1H, s, NH);  $^{13}\text{C}$  NMR (100.6 MHz,  $\text{CDCl}_3$ )  $\delta$  = 24.05, 28.01, 35.18, 50.70, 70.66, 116.04, 117.38, 127.74,

128.63, 128.86, 135.26, 137.09, 141.29, 144.52, 153.99. HRMS (ES<sup>+</sup>): m/z calculated for C<sub>20</sub>H<sub>25</sub>N<sub>3</sub>O<sub>2</sub>: 362.1845 [M+Na]<sup>+</sup>. Found 362.1846.

### **1-(3-(benzyloxy)pyridin-2-yl)-3-(tert-butyl)urea (5b)**

White solid, yield: 21%, mp: 78–79 °C, HPLC purity: 1.90 min, 99.54%, <sup>1</sup>H NMR (400 MHz, CDCl<sub>3</sub>) δ = 1.44 (9H, s, 3CH<sub>3</sub>), 5.09 (2H, s, OCH<sub>2</sub>Ph), 6.77 (1H, dd, *J* = 5.1 Hz, 8.0 Hz, ArH), 7.05 (1H, dd, *J* = 1.3 Hz, 8.0 Hz, ArH), 7.23 (1H, s, NH), 7.35–7.39 (5H, m, ArH), 7.74 (1H, dd, *J* = 1.3 Hz, 5.1 Hz, ArH), 9.46 (1H, s, NH); <sup>13</sup>C NMR (100.6 MHz, CDCl<sub>3</sub>) δ = 29.18, 50.42, 70.60, 115.90, 117.31, 127.64, 128.58, 128.83, 135.32, 137.02, 141.20, 144.59, 153.60. HRMS (ES<sup>+</sup>): m/z calculated for C<sub>17</sub>H<sub>21</sub>N<sub>3</sub>O<sub>2</sub>: 322.1532 [M+Na]<sup>+</sup>. Found 322.1529.

### **1-(3-(3-fluorobenzyloxy)pyridin-2-yl)-3-cycloheptylurea (5c)**

White solid, yield: 71%, mp: 186–189 °C, HPLC purity: 8.30 min, 94.48%, <sup>1</sup>H NMR (400 MHz, CDCl<sub>3</sub>) δ = 1.57–1.68 (10H, m, 5CH<sub>2</sub>), 1.95–2.01 (2H, m, CH<sub>2</sub>), 4.02–4.04 (1H, m, CH), 5.08 (2H, s, OCH<sub>2</sub>Ph), 6.78 (1H, dd, *J* = 5.1 Hz, 8.0 Hz, ArH), 7.03 (1H, dd, *J* = 1.3 Hz, 8.0 Hz, ArH), 7.06–7.09 (2H, m, ArH), 7.16 (1H, d, *J* = 7.7 Hz, ArH), 7.31 (1H, s, NH), 7.34–7.39 (1H, m, ArH), 7.78 (1H, dd, *J* = 1.3 Hz, 5.1 Hz, ArH), 9.51 (1H, s, NH); <sup>13</sup>C NMR (100.6 MHz, CDCl<sub>3</sub>) δ = 29.59, 36.54, 42.02, 42.58, 51.09, 69.81, 114.52 (*J*<sub>C-F</sub> = 22.0 Hz), 115.56 (*J*<sub>C-F</sub> = 21.0 Hz), 115.79, 117.34, 122.96, 130.52 (*J*<sub>C-F</sub> = 8.1 Hz), 137.29, 137.75, 140.96, 144.63, 153.12, 162.96 (*J*<sub>C-F</sub> = 245.9 Hz). HRMS (ES<sup>+</sup>): m/z calculated for C<sub>17</sub>H<sub>21</sub>N<sub>3</sub>O<sub>2</sub>: 396.2836 [M+K]<sup>+</sup>. Found 396.2121.

### **1-(3-(3-fluorobenzyloxy)pyridin-2-yl)-3-(2,4,4-trimethylpentan-2-yl)urea (5d)**

White solid, yield: 18%, mp: 107–111 °C,  $^1\text{H}$  NMR (400 MHz,  $\text{CDCl}_3$ )  $\delta$  = 1.05 (9H, s, 3 $\text{CH}_3$ ), 1.49 (6H, s, 2 $\text{CH}_3$ ), 1.82 (2H, s,  $\text{CH}_2$ ), 5.07 (2H, s,  $\text{OCH}_2\text{Ph}$ ), 6.77 (1H, dd,  $J$  = 5.1 Hz, 7.9 Hz, ArH), 7.02 (1H, dd,  $J$  = 1.2 Hz, 7.9 Hz, ArH), 7.04–7.09 (2H, m, ArH), 7.16 (1H, d,  $J$  = 7.7 Hz, ArH), 7.18 (1H, s, NH), 7.33–7.37 (1H, m, ArH), 7.75 (1H, dd,  $J$  = 1.2 Hz, 5.1 Hz, ArH), 9.50 (1H, s, NH);  $^{13}\text{C}$  NMR (100.6 MHz,  $\text{CDCl}_3$ )  $\delta$  = 29.69, 30.23, 31.50, 31.57, 31.66, 51.83, 52.07, 54.19, 69.82, 114.49 ( $J_{\text{C-F}}$  = 21.9 Hz), 115.55 ( $J_{\text{C-F}}$  = 20.9 Hz), 115.82, 117.29, 123.04, 130.52 ( $J_{\text{C-F}}$  = 8.1 Hz), 137.24, 137.80, 140.87, 144.53, 153.33, 162.97 ( $J_{\text{C-F}}$  = 245.9 Hz). HRMS ( $\text{ES}^+$ ):  $m/z$  calculated for  $\text{C}_{21}\text{H}_{28}\text{FN}_3\text{O}_2$ : 396.2064 [ $\text{M}+\text{Na}$ ] $^+$ . Found 396.2060.

#### **1-(3-(3-fluorobenzyloxy)pyridin-2-yl)-3-ethylurea (5e)**

Yellow solid, yield: 39%, mp: 55–56 °C, HPLC purity: 4.08 min, 95.66%,  $^1\text{H}$  NMR (400 MHz,  $\text{CDCl}_3$ )  $\delta$  = 1.25 (3H, t,  $J$  = 7.2 Hz,  $\text{CH}_3$ ), 3.40–3.44 (2H, m,  $\text{CH}_2$ ), 5.08 (2H, s,  $\text{OCH}_2\text{Ph}$ ), 6.79 (1H, dd,  $J$  = 5.1 Hz, 8.0 Hz, ArH), 7.03–7.08 (3H, m, ArH), 7.16 (1H, d,  $J$  = 7.6 Hz, ArH), 7.34–7.38 (2H, m, ArH+NH), 7.77–7.78 (1H, m, ArH), 9.42 (1H, s, NH);  $^{13}\text{C}$  NMR (100.6 MHz,  $\text{CDCl}_3$ )  $\delta$  = 15.37, 34.71, 69.89, 114.60 ( $J_{\text{C-F}}$  = 21.9 Hz), 115.62 ( $J_{\text{C-F}}$  = 21.1 Hz), 116.20, 117.48, 123.14, 130.56 ( $J_{\text{C-F}}$  = 8.1 Hz), 137.37, 137.66, 141.02, 144.31, 154.87, 162.99 ( $J_{\text{C-F}}$  = 245.9 Hz). HRMS ( $\text{ES}^+$ ):  $m/z$  calculated for  $\text{C}_{15}\text{H}_{16}\text{FN}_3\text{O}_2$ : 312.1125 [ $\text{M}+\text{Na}$ ] $^+$ . Found 312.1118.

#### **1-(3-(3-fluorobenzyloxy)pyridin-2-yl)-3-(*tert*-butyl)urea (5f)**

White solid, yield: 32%, mp: 108–109 °C, HPLC purity: 2.02 min, 99.93%,  $^1\text{H}$  NMR (400 MHz,  $\text{CDCl}_3$ )  $\delta$  = 1.46 (9H, s, 3 $\text{CH}_3$ ), 5.08 (2H, s,  $\text{OCH}_2\text{Ph}$ ), 6.77 (1H, dd,  $J$  = 5.1 Hz, 8.0 Hz, ArH), 7.02 (1H, dd,  $J$  = 1.3 Hz, 8.0 Hz, ArH), 7.04–7.09 (2H, m, ArH), 7.16 (1H, d,  $J$  = 7.6 Hz, ArH),

7.20 (1H, s, NH), 7.33–7.39 (1H, m, ArH), 7.75 (1H, dd,  $J = 1.3$  Hz, 5.1 Hz, ArH), 9.5 (1H, s, NH);  $^{13}\text{C}$  NMR (100.6 MHz,  $\text{CDCl}_3$ )  $\delta = 29.17, 50.45, 69.80, 114.46$  ( $J_{\text{C-F}} = 21.9$  Hz), 115.54 ( $J_{\text{C-F}} = 21.0$  Hz), 115.86, 117.34, 123.01, 130.51 ( $J_{\text{C-F}} = 8.1$  Hz), 137.31, 137.81, 140.91, 144.56, 153.52, 162.98 ( $J_{\text{C-F}} = 245.9$  Hz). HRMS ( $\text{ES}^+$ ):  $m/z$  calculated for  $\text{C}_{17}\text{H}_{20}\text{FN}_3\text{O}_2$ : 340.1438  $[\text{M}+\text{Na}]^+$ . Found 340.1434.

### **1-(3-(2-chlorobenzoyloxy)pyridin-2-yl)-3-cycloheptylurea (5g)**

White solid, yield: 72%, mp: 120–121 °C, HPLC purity: 6.99 min, 96.82%,  $^1\text{H}$  NMR (400 MHz,  $\text{CDCl}_3$ )  $\delta = 1.56$ – $1.68$  (10H, m,  $5\text{CH}_2$ ), 1.97–1.98 (2H, m,  $\text{CH}_2$ ), 4.01–4.05 (1H, m, CH), 5.20 (2H, s,  $\text{OCH}_2\text{Ph}$ ), 6.81 (1H, dd,  $J = 5.1$  Hz, 8.0 Hz, ArH), 7.07 (1H, dd,  $J = 1.3$  Hz, 8.0 Hz, ArH), 7.28–7.32 (2H, m, ArH), 7.33 (1H, s, NH), 7.41–7.44 (2H, m, ArH), 7.78 (1H, dd,  $J = 1.3$  Hz, ArH), 9.52 (1H, s, NH);  $^{13}\text{C}$  NMR (100.6 MHz,  $\text{CDCl}_3$ )  $\delta = 24.05, 28.01, 35.18, 50.72, 67.82, 116.11, 117.51, 127.27, 129.34, 129.76, 129.87, 132.95, 133.20, 137.39, 141.04, 144.48, 153.95$ . HRMS ( $\text{ES}^+$ ):  $m/z$  calculated for  $\text{C}_{20}\text{H}_{24}\text{ClN}_3\text{O}_2$ : 396.1455  $[\text{M}+\text{Na}]^+$ . Found 396.1448.

### **1-(3-(2-chlorobenzoyloxy)pyridin-2-yl)-3-(2,4,4-trimethylpentan-2-yl)urea (5h)**

Pink solid, yield: 90%, mp: 110–112 °C,  $^1\text{H}$  NMR (400 MHz,  $\text{CDCl}_3$ )  $\delta = 1.03$  (9H, s,  $3\text{CH}_3$ ), 1.49 (6H, s,  $2\text{CH}_3$ ), 1.82 (2H, s,  $\text{CH}_2$ ), 5.19 (2H, s,  $\text{OCH}_2\text{Ph}$ ), 6.79 (1H, dd,  $J = 5.1$  Hz, 8.0 Hz, ArH), 7.04 (1H, dd,  $J = 1.3$  Hz, 8.0 Hz, ArH), 7.21 (1H, s, NH), 7.29–7.32 (2H, m, ArH), 7.41–7.45 (2H, m, ArH), 7.75 (1H, dd,  $J = 1.3$  Hz, 5.1 Hz, ArH), 9.51 (1H, s, NH);  $^{13}\text{C}$  NMR (100.6 MHz,  $\text{CDCl}_3$ )  $\delta = 29.69, 31.51, 31.66, 51.87, 54.19, 67.75, 115.91, 117.44, 127.25, 129.19, 129.70, 129.78, 133.03, 137.26, 140.90, 144.55, 153.37$ . HRMS ( $\text{ES}^+$ ):  $m/z$  calculated for  $\text{C}_{21}\text{H}_{28}\text{ClN}_3\text{O}_2$ : 412.1768  $[\text{M}+\text{Na}]^+$ . Found 412.1761.

**1-(3-(2-chlorobenzyloxy)pyridin-2-yl)-3-ethylurea (5i)**

White solid, yield: 91%, mp: 84–85 °C, HPLC purity: 1.71 min, 99.90%, <sup>1</sup>H NMR (400 MHz, CDCl<sub>3</sub>) δ = 1.25 (3H, t, *J* = 7.24 Hz, CH<sub>3</sub>), 3.39–3.46 (2H, m, CH<sub>2</sub>), 5.20 (2H, s, OCH<sub>2</sub>Ph), 6.79 (1H, dd, *J* = 5.1 Hz, 8.0 Hz, ArH), 7.04 (1H, dd, *J* = 1.3 Hz, 8.0 Hz, ArH), 7.30–7.34 (2H, m, ArH), 7.38 (1H, s, NH), 7.41–7.44 (2H, m, ArH), 7.78 (1H, dd, *J* = 1.3 Hz, 5.1 Hz, ArH), 9.42 (1H, s, NH); <sup>13</sup>C NMR (100.6 MHz, CDCl<sub>3</sub>) δ = 15.39, 34.70, 67.86, 116.29, 117.58, 127.26, 129.39, 129.76, 129.90, 132.89, 133.26, 137.36, 141.04, 144.29, 154.87. HRMS (ES<sup>+</sup>): *m/z* calculated for C<sub>15</sub>H<sub>16</sub>ClN<sub>3</sub>O<sub>2</sub>: 328.0829 [M+Na]<sup>+</sup>. Found 328.0825.

**1-(3-(3-chlorobenzyloxy)pyridin-2-yl)-3-cycloheptylurea (5j)**

Yellow oil, yield: 69%, HPLC purity: 6.52 min, 98.61%, <sup>1</sup>H NMR (400 MHz, CDCl<sub>3</sub>) δ = 1.56–1.67 (10H, m, 5CH<sub>2</sub>), 1.97–2.04 (2H, m, CH<sub>2</sub>), 4.01–4.03 (1H, m, CH), 5.06 (2H, s, OCH<sub>2</sub>Ph), 6.79 (1H, dd, *J* = 5.1 Hz, 8.0 Hz, ArH), 7.02 (1H, dd, *J* = 1.3 Hz, 8.0 Hz, ArH), 7.27–7.28 (1H, m, ArH), 7.30 (1H, s, NH), 7.33–7.36 (3H, m, ArH), 7.78 (1H, dd, *J* = 1.3 Hz, 5.1 Hz, ArH), 9.52 (1H, s, NH); <sup>13</sup>C NMR (100.6 MHz, CDCl<sub>3</sub>) δ = 24.05, 28.01, 35.17, 50.74, 69.84, 116.03, 117.40, 125.70, 127.73, 128.84, 130.23, 134.79, 137.27, 137.42, 140.98, 144.46, 153.91. HRMS (ES<sup>+</sup>): *m/z* calculated for C<sub>20</sub>H<sub>24</sub>ClN<sub>3</sub>O<sub>2</sub>: 396.1455 [M+Na]<sup>+</sup>. Found 396.1443.

**1-(3-(3-chlorobenzyloxy)pyridin-2-yl)-3-(2,4,4-trimethylpentan-2-yl)urea (5k)**

Yellow solid, yield: 84%, mp: 109–110 °C, <sup>1</sup>H NMR (400 MHz, CDCl<sub>3</sub>) δ = 1.03 (9H, s, 3CH<sub>3</sub>), 1.49 (6H, s, 2CH<sub>3</sub>), 1.81 (2H, s, CH<sub>2</sub>), 5.05 (2H, s, OCH<sub>2</sub>Ph), 6.77 (1H, dd, *J* = 5.1 Hz, 8.0 Hz, ArH), 7.01 (1H, dd, *J* = 1.3 Hz, 8.0 Hz, ArH), 7.17 (1H, s, NH), 7.27–7.28 (1H, m, ArH),

7.32–7.36 (3H, m, ArH), 7.75 (1H, dd,  $J = 1.3$  Hz, 5.1 Hz, ArH), 9.50 (1H, s, NH);  $^{13}\text{C}$  NMR (100.6 MHz,  $\text{CDCl}_3$ )  $\delta = 29.68, 31.51, 31.66, 51.85, 54.19, 69.80, 115.82, 117.29, 125.63, 127.65, 128.79, 130.20, 134.76, 137.27, 140.85, 144.52, 153.32$ . HRMS ( $\text{ES}^+$ ):  $m/z$  calculated for  $\text{C}_{21}\text{H}_{28}\text{ClN}_3\text{O}_2$ : 412.1768  $[\text{M}+\text{Na}]^+$ . Found 412.1762.

### **1-(3-(3-chlorobenzyloxy)pyridin-2-yl)-3-(tert-butyl)urea (5l)**

Yellow solid, yield: 33%, mp: 99–101 °C, HPLC purity: 2.52 min, 92.98%,  $^1\text{H}$  NMR (400 MHz,  $\text{CDCl}_3$ )  $\delta = 1.44$  (9H, s, 3 $\text{CH}_3$ ), 5.06 (2H, s,  $\text{OCH}_2\text{Ph}$ ), 6.77 (1H, dd,  $J = 5.1$  Hz, 8.0 Hz, ArH), 7.01 (1H, dd,  $J = 1.3$  Hz, 8.0 Hz, ArH), 7.19 (1H, s, NH), 7.27–7.36 (4H, m, ArH), 7.76 (1H, dd,  $J = 1.3$  Hz, 5.1 Hz, ArH), 9.44 (1H, s, NH);  $^{13}\text{C}$  NMR (100.6 MHz,  $\text{CDCl}_3$ )  $\delta = 29.17, 50.45, 67.78, 115.89, 117.35, 125.60, 127.62, 128.78, 130.20, 134.76, 137.33, 140.89, 144.52, 153.53$ . HRMS ( $\text{ES}^+$ ):  $m/z$  calculated for  $\text{C}_{17}\text{H}_{20}\text{ClN}_3\text{O}_2$ : 356.1142  $[\text{M}+\text{Na}]^+$ . Found 356.1136.

### **1-(3-(4-chlorobenzyloxy)pyridin-2-yl)-3-cycloheptylurea (5m)**

White solid, yield: 55%, mp: 118–119 °C, HPLC purity: 6.08 min, 98.58%,  $^1\text{H}$  NMR (400 MHz,  $\text{CDCl}_3$ )  $\delta = 1.58$ – $1.67$  (10H, m, 5 $\text{CH}_2$ ), 1.97–1.98 (2H, m,  $\text{CH}_2$ ), 4.00–4.04 (1H, m, CH), 5.06 (2H, s,  $\text{OCH}_2\text{Ph}$ ), 6.81 (1H, dd,  $J = 5.2$  Hz, 8.0 Hz, ArH), 7.03 (1H, dd,  $J = 1.2$  Hz, 8.0 Hz, ArH), 7.31 (3H, m, ArH+NH), 7.37 (2H, d,  $J = 8.4$  Hz, ArH), 7.77 (1H, dd,  $J = 1.2$  Hz, 5.2 Hz, ArH), 9.52 (1H, s, NH). HRMS ( $\text{ES}^+$ ):  $m/z$  calculated for  $\text{C}_{20}\text{H}_{24}\text{ClN}_3\text{O}_2$ : 396.1455  $[\text{M}+\text{Na}]^+$ . Found 396.1446.

### **1-(3-(4-chlorobenzyloxy)pyridin-2-yl)-3-ethylurea (5n)**

White solid, yield: 47%, mp: 83–84 °C, HPLC purity: 1.58 min, 99.63%, <sup>1</sup>H NMR (300 MHz, DMSO-*d*<sub>6</sub>) δ = 1.10 (3H, t, *J* = 7.2 Hz, CH<sub>3</sub>), 3.22–3.29 (2H, m, CH<sub>2</sub>), 5.21 (2H, s, OCH<sub>2</sub>Ph), 6.93 (1H, dd, *J* = 5.1 Hz, 8.1 Hz, ArH), 7.43 (1H, d, *J* = 8.1 Hz, ArH), 7.47 (2H, d, *J* = 8.4 Hz, ArH), 7.54 (2H, d, *J* = 8.4 Hz, ArH), 7.69 (1H, s, NH), 7.79 (1H, d, *J* = 5.1 Hz, ArH), 9.21 (1H, s, NH). <sup>13</sup>C NMR (100.6 MHz, DMSO-*d*<sub>6</sub>) δ = 15.80, 34.47, 69.49, 117.17, 119.34, 128.94, 130.22, 133.33, 135.52, 137.44, 141.32, 144.26, 145.35. HRMS (ES<sup>+</sup>): *m/z* calculated for C<sub>15</sub>H<sub>16</sub>ClN<sub>3</sub>O<sub>2</sub>: 328.0829 [M+Na]<sup>+</sup>. Found 328.0817.

### 1-(3-(4-chlorobenzyloxy)pyridin-2-yl)-3-(*tert*-butyl)urea (5o)

White solid, yield: 35%, mp: 112–113 °C, HPLC purity: 2.71 min, 98.32%, <sup>1</sup>H NMR (400 MHz, CDCl<sub>3</sub>) δ = 1.57 (9H, s, 3CH<sub>3</sub>), 5.10 (2H, s, OCH<sub>2</sub>Ph), 6.77 (1H, dd, *J* = 5.2 Hz, 8.0 Hz, ArH), 7.12 (1H, dd, *J* = 1.2 Hz, 8.0 Hz, ArH), 7.33 (2H, d, *J* = 8.4 Hz, ArH), 7.40 (2H, d, *J* = 8.4 Hz, ArH), 7.50 (1H, s, NH), 7.87 (1H, dd, *J* = 1.2 Hz, 5.2 Hz, ArH), 11.97 (1H, s, NH). <sup>13</sup>C NMR (100.6 MHz, CDCl<sub>3</sub>) δ = 29.34, 50.14, 69.50, 117.06, 119.35, 128.99, 130.27, 133.31, 135.55, 137.36, 141.26, 144.37, 153.02. HRMS (ES<sup>+</sup>): *m/z* calculated for C<sub>17</sub>H<sub>20</sub>ClN<sub>3</sub>O<sub>2</sub>: 356.1142 [M+Na]<sup>+</sup>. Found 356.1133.

### 1-(3-(4-fluorobenzyloxy)pyridin-2-yl)-3-cycloheptylurea (5p)

Yellow solid, yield: 47%, mp: 110–113 °C, HPLC purity: 3.97 min, 94.72%, <sup>1</sup>H NMR (400 MHz, CDCl<sub>3</sub>) δ = 1.58–1.65 (10H, m, CH<sub>2</sub>), 1.96–1.99 (2H, m, CH<sub>2</sub>), 4.01–4.04 (1H, m, CH), 5.04 (2H, s, OCH<sub>2</sub>Ph), 6.79 (1H, dd, *J* = 4.8 Hz, 8.0 Hz, ArH), 7.04–7.11 (3H, m, ArH), 7.30 (1H, s, NH), 7.34–7.37 (2H, m, ArH), 7.77 (1H, d, *J* = 4.8 Hz, ArH), 9.52 (1H, s, NH). HRMS (ES<sup>+</sup>): *m/z* calculated for C<sub>20</sub>H<sub>24</sub>FN<sub>3</sub>O<sub>2</sub>: 380.1751 [M+Na]<sup>+</sup>. Found 380.1742.

**1-(3-(4-fluorobenzyloxy)pyridin-2-yl)-3-ethylurea (5q)**

White solid, yield: 44%, mp: 85–86 °C, HPLC purity: 1.23 min, 95.91%, <sup>1</sup>H NMR (400 MHz, CDCl<sub>3</sub>) δ = 1.24 (3H, t, *J* = 7.2 Hz, CH<sub>3</sub>), 3.38–3.45 (2H, m, CH<sub>2</sub>), 5.04 (2H, s, OCH<sub>2</sub>Ph), 6.80 (1H, dd, *J* = 5.2 Hz, 8.0 Hz, ArH), 7.05–7.12 (3H, m, ArH), 7.34–7.38 (3H, m, ArH+NH), 7.77 (1H, dd, *J* = 1.2 Hz, 5.2 Hz, ArH), 9.41 (1H, s, NH). HRMS (ES<sup>+</sup>): *m/z* calculated for C<sub>15</sub>H<sub>16</sub>FN<sub>3</sub>O<sub>2</sub>: 312.1125 [M+Na]<sup>+</sup>. Found 312.1115.

**1-(3-(4-fluorobenzyloxy)pyridin-2-yl)-3-(*tert*-butyl)urea (5r)**

Light yellow solid, yield: 54%, mp: 98–99 °C, HPLC purity: 1.90 min, 98.60%, <sup>1</sup>H NMR (400 MHz, CDCl<sub>3</sub>) δ = 1.44 (9H, s, 3CH<sub>3</sub>), 5.04 (2H, s, OCH<sub>2</sub>Ph), 6.77 (1H, dd, *J* = 4.8 Hz, 8.0 Hz, ArH), 7.03–7.08 (3H, m, ArH), 7.10 (1H, s, NH), 7.34–7.37 (2H, m, ArH), 7.74 (1H, dd, *J* = 1.2 Hz, 4.8 Hz, ArH), 9.44 (1H, s, NH). HRMS (ES<sup>+</sup>): *m/z* calculated for C<sub>17</sub>H<sub>20</sub>FN<sub>3</sub>O<sub>2</sub>: 340.1438 [M+Na]<sup>+</sup>. Found 340.1428.

**4.1.3. General procedure of urea compounds (5s–w)**

2-amino-3-benzyloxy pyridine derivative (200 mg, 0.92 mmol) and DIPEA (0.5 mL, 2.87 mmol) were dissolved in dry THF (5 mL), 2-chloroethyl isocyanate (0.1 mL, 1.2 mmol) was added to the reaction mixture. The reaction was refluxed for 18 h. After cooling, the reaction mixture was evaporated and the residue was purified by flash column chromatography (SiO<sub>2</sub>, EA/*n*-Hex = 1/4).

**1-(3-(benzyloxy)pyridin-2-yl)-3-chloroethylurea (5s)**

White solid, yield: 97%, mp: 72–73 °C,  $^1\text{H}$  NMR (400 MHz,  $\text{CDCl}_3$ )  $\delta$  = 3.69–6.74 (4H, m, 2 $\text{CH}_2$ ), 5.10 (2H,  $\text{OCH}_2\text{Ph}$ ), 6.83 (1H, dd,  $J$  = 5.1 Hz, 8.0 Hz, ArH), 7.10 (1H, dd,  $J$  = 1.3 Hz, 8.0 Hz, ArH), 7.36–7.44 (6H, m, ArH+NH), 7.79 (1H, dd,  $J$  = 1.3 Hz, 5.1 Hz, ArH), 9.91 (1H, s, NH);  $^{13}\text{C}$  NMR (100.6 MHz,  $\text{CDCl}_3$ )  $\delta$  = 41.85, 44.02, 70.76, 116.64, 117.71, 127.80, 128.72, 128.90, 135.12, 137.18, 141.39, 143.95, 155.05. HRMS ( $\text{ES}^+$ ):  $m/z$  calculated for  $\text{C}_{15}\text{H}_{16}\text{ClN}_3\text{O}_2$ : 328.0829  $[\text{M}+\text{Na}]^+$ . Found 328.0818.

#### **1-(3-(3-chlorobenzoyloxy)pyridin-2-yl)-3-chloroethylurea (5t)**

White solid, yield: 88%, mp: 110–111 °C, HPLC purity: 1.76 min, 91.52%,  $^1\text{H}$  NMR (400 MHz,  $\text{CDCl}_3$ )  $\delta$  = 3.69–6.74 (4H, m, 2 $\text{CH}_2$ ), 5.07 (2H,  $\text{OCH}_2\text{Ph}$ ), 6.83 (1H, dd,  $J$  = 5.1 Hz, 8.0 Hz, ArH), 7.06 (1H, dd,  $J$  = 1.3 Hz, 8.0 Hz, ArH), 7.27–7.36 (4H, m, ArH), 7.41 (1H, s, NH), 7.81 (1H, dd,  $J$  = 1.3 Hz, 5.1 Hz, ArH), 9.90 (1H, s, NH);  $^{13}\text{C}$  NMR (100.6 MHz,  $\text{CDCl}_3$ )  $\delta$  = 41.86, 44.00, 69.92, 116.63, 117.72, 125.76, 127.78, 128.90, 130.25, 134.80, 137.15, 137.51, 141.06, 143.89, 154.95. HRMS ( $\text{ES}^+$ ):  $m/z$  calculated for  $\text{C}_{15}\text{H}_{15}\text{Cl}_2\text{N}_3\text{O}_2$ : 362.0439  $[\text{M}+\text{Na}]^+$ . Found 362.0475.

#### **1-(3-(2-chlorobenzoyloxy)pyridin-2-yl)-3-chloroethylurea (5u)**

White solid, yield: 61%, mp: 114–115 °C, HPLC purity: 1.92 min, 92.55%,  $^1\text{H}$  NMR (400 MHz,  $\text{CDCl}_3$ )  $\delta$  = 3.69–6.76 (4H, m, 2 $\text{CH}_2$ ), 5.20 (2H,  $\text{OCH}_2\text{Ph}$ ), 6.83 (1H, dd,  $J$  = 5.1 Hz, 8.0 Hz, ArH), 7.06 (1H, dd,  $J$  = 1.3 Hz, 8.0 Hz, ArH), 7.30–7.34 (2H, m, ArH) 7.41–7.45 (3H, m, ArH+NH), 7.81 (1H, dd,  $J$  = 1.3 Hz, 5.1 Hz, ArH), 9.91 (1H, s, NH);  $^{13}\text{C}$  NMR (100.6 MHz,  $\text{CDCl}_3$ )  $\delta$  = 41.87, 44.02, 67.97, 116.70, 117.82, 127.24, 129.42, 129.82, 129.98, 132.83, 133.32,

137.44, 141.13, 143.94, 154.99. HRMS (ES<sup>+</sup>): m/z calculated for C<sub>15</sub>H<sub>15</sub>Cl<sub>2</sub>N<sub>3</sub>O<sub>2</sub>: 362.0439 [M+Na]<sup>+</sup>. Found 362.0445.

#### **1-(3-(4-chlorobenzyloxy)pyridin-2-yl)-3-chloroethylurea (5v)**

White solid, yield: 70%, mp: 109–110 °C, HPLC purity: 1.76 min, 90.35%, <sup>1</sup>H NMR (400 MHz, CDCl<sub>3</sub>) δ = 3.69–3.74 (4H, m, 2CH<sub>2</sub>), 5.07 (2H, s, OCH<sub>2</sub>Ph), 6.83 (1H, dd, *J* = 4.8 Hz, 8.0 Hz, ArH), 7.07 (1H, d, *J* = 8.0 Hz, ArH), 7.32 (2H, d, *J* = 8.4 Hz, ArH), 7.38 (3H, d, *J* = 8.4 Hz, ArH+NH), 7.80 (1H, d, *J* = 4.8 Hz, ArH), 9.89 (1H, s, NH). HRMS (ES<sup>+</sup>): m/z calculated for C<sub>15</sub>H<sub>15</sub>Cl<sub>2</sub>N<sub>3</sub>O<sub>2</sub>: 362.0439 [M+Na]<sup>+</sup>. Found 362.0443.

#### **1-(3-(4-fluorobenzyloxy)pyridin-2-yl)-3-chloroethylurea (5w)**

White solid, yield: 74%, mp: 80–82 °C, <sup>1</sup>H NMR (400 MHz, CDCl<sub>3</sub>) δ = 3.63–3.73 (4H, m, 2CH<sub>2</sub>), 5.05 (2H, s, OCH<sub>2</sub>Ph), 6.83 (1H, dd, *J* = 5.2 Hz, 8.0 Hz, ArH), 7.07–7.12 (3H, m, ArH), 7.35–7.39 (3H, m, ArH+NH), 7.80 (1H, d, *J* = 5.2 Hz, ArH), 9.90 (1H, s, NH). HRMS (ES<sup>+</sup>): m/z calculated for C<sub>15</sub>H<sub>15</sub>ClFN<sub>3</sub>O<sub>2</sub>: 346.0735 [M+Na]<sup>+</sup>. Found 346.0796.

#### **4.1.4. General procedure of urea compounds 5x and 5y:**

Potassium carbonate (407 mg, 2.95 mmol) and piperazine (169 mg, 1.96 mmol) were dissolved in the solution of 1-(3-(benzyloxy)pyridin-2-yl)-3-ethylurea derivative in acetonitrile (5 mL). The reaction mixture was refluxed for 20 h. After cooling, the reaction mixture was quenched by addition of water. The mixture was extracted with ethyl acetate. The organic layer was dried over Na<sub>2</sub>SO<sub>4</sub>, filtered and concentrated under reduced pressure. The residue was purified by flash column chromatography (SiO<sub>2</sub>, DCM/MeOH = 5/1) to give the title compounds.

**1-(3-(benzyloxy)pyridin-2-yl)-3-(2-(piperazin-1-yl)ethyl)urea (5x)**

Light yellow solid, yield: 19%, mp: 154–159 °C,  $^1\text{H}$  NMR (400 MHz,  $\text{CDCl}_3$ )  $\delta$  = 2.49 (4H, brs, 2 $\text{CH}_2$ ), 2.58 (2H, t,  $J$  = 6.4 Hz,  $\text{CH}_2$ ), 2.91–2.93 (4H, m, 2 $\text{CH}_2$ ), 3.49–3.53 (2H, m,  $\text{CH}_2$ ), 5.09 (2H, s,  $\text{OCH}_2\text{Ph}$ ), 6.81 (1H, dd,  $J$  = 5.2 Hz, 8.0 Hz, ArH), 7.09 (1H, d,  $J$  = 8.0 Hz, ArH), 7.35–7.40 (5H, m, ArH), 7.42 (1H, s, NH), 7.78 (1H, d,  $J$  = 5.2 Hz, ArH), 9.72 (1H, s, NH);  $^{13}\text{C}$  NMR (100.6 MHz,  $\text{CDCl}_3$ )  $\delta$  = 36.88, 44.00, 49.89, 51.51, 52.83, 57.02, 70.74, 116.34, 117.51, 127.75, 128.68, 128.87, 135.16, 137.18, 141.37, 144.22, 154.97.

**1-(3-(3-chlorobenzyloxy)pyridin-2-yl)-3-(2-(piperazin-1-yl)ethyl)urea (5y)**

Colorless oil, yield: 22%,  $^1\text{H}$  NMR (400 MHz,  $\text{CDCl}_3$ )  $\delta$  = 2.52 (4H, brs, 2 $\text{CH}_2$ ), 2.58 (2H, t,  $J$  = 6.4 Hz,  $\text{CH}_2$ ), 2.94 (4H, t,  $J$  = 4.8 Hz, 2 $\text{CH}_2$ ), 3.49–3.53 (2H, m,  $\text{CH}_2$ ), 5.07 (2H, s,  $\text{OCH}_2\text{Ph}$ ), 6.81 (1H, dd,  $J$  = 4.8 Hz, 8.0 Hz, ArH), 7.04 (1H, dd,  $J$  = 1.2 Hz, 8.0 Hz, ArH), 7.27–7.28 (1H, m, ArH), 7.33–7.37 (4H, m, ArH+NH), 7.81 (1H, dd,  $J$  = 1.2 Hz, 4.8 Hz, ArH), 9.72 (1H, s, NH).

**4.2. Biological evaluation****4.2.1. JC-1 assay (Mitochondrial membrane potential assay)**

HT-22 cells (30,000 per well) were seeded into a clear 96-well plate (FALCON) at 200  $\mu\text{L}$  per well one day prior to assay. 750  $\mu\text{M}$  of JC-1 (Stratagene) in DMSO stock solution was dissolved into phenol red-free Opti-MEM (GIBCO) medium to make final concentration of 7.5  $\mu\text{M}$  JC-1 per well. Medium was removed from the plate, and 100  $\mu\text{L}$  per well of JC-1 was added. Plates were incubated for 1 h and 15 min at 37 °C and washed twice with 100  $\mu\text{L}$  per well PBS.

Subsequently, cells were treated with 25  $\mu$ L solution of each compound at 5  $\mu$ M in Opti-MEM and incubated at 37 °C for 10 min followed by addition of 25  $\mu$ L of A $\beta$  (American peptide, 1–42) solution at 5  $\mu$ M. Fluorescence was measured at every 1 h for 3 h at ex/em 530 nm/580 nm ('red') and ex/em 485 nm/530 nm ('green'). The ratio of green to red fluorescence was recorded and the percent changes in ratio from each compound were calculated and normalized using vehicle control as 100%.

#### **4.2.2. Compound's Induction of ROS production assay**

Neuro-2a human neuroblastoma cells (from American Type Culture Collection, Manassas, VA) were grown in EMEM medium supplemented with 10% fetal bovine serum (FBS), 100  $\mu$ g/ml penicillin, and 100  $\mu$ g/ml streptomycin and maintained at 37°C under a humidified atmosphere of 5% CO<sub>2</sub> and 95% air. 10 mM stock solution of compounds to be tested and standard Menadione in DMSO were diluted 3-fold in 10 doses with DMSO. To 25 nL of the prepared solutions in the wells of the 384-well culture plate, 25  $\mu$ L of culture medium containing 2000 of Neuro-2a cells was added. 4  $\mu$ L of H<sub>2</sub>O<sub>2</sub> substrate solution was immediately added to the cells, mixed and the culture mixture was incubated at 37°C, 5% CO<sub>2</sub> for 6 hours. After addition of 30  $\mu$ L of ROS-Glo™ detection solution and incubated at room temperature for 20 minutes, luminescence was measured by Envision 2104 Multi label Reader (PerkinElmer, Santa Clara, CA). Bar graphs for compounds vs. H<sub>2</sub>O<sub>2</sub> production were plotted using the GraphPad Prism 4 program for calculation of IC<sub>50</sub>.

#### **4.2.3. Compound's Induction of cytotoxicity assay**

Neuro-2a human neuroblastoma cell culture was grown as mentioned previously. 10 mM stock solution of compounds to be tested and standard staurosporine (Sigma-Aldrich Saint Louis, MI) were prepared and diluted as mentioned previously. To 25 nL of the prepared solutions in the wells of the 384-well culture plate, 25  $\mu$ L of culture medium containing 2000 of Neuro-2a cells was added. Culture mixtures were incubated at 37°C, 5% CO<sub>2</sub> for 72 hours, then 5  $\mu$ L of MTT solution (CellTiter 96® Non-Radioactive Cell Proliferation Assay, Promega, Madison, WI) was added to each well and incubated at 37°C in a CO<sub>2</sub> incubator for further 4 hours. After formation of the formazan, 25  $\mu$ L of solubilization /stop solution was added and the plate was incubated for another 1 hour at 37°C in a CO<sub>2</sub> incubator to dissolve the formazan crystals. The absorbance was measured at 590 nm using Envision 2104 Multilabel Reader (PerkinElmer, Santa Clara, CA). The cell viability was determined based on the quantification of the color intensity in each culture well and the IC<sub>50</sub> values were calculated using the GraphPad Prism 4 program based on a sigmoidal dose-response equation.

#### **4.2.4. Assay for cellular ATP levels (Luciferase-based assay)**

10,000 HT-22 cells per well were seeded into a clear 96-well plate (FALCON) at 200  $\mu$ L per well one day prior to assay. Medium was removed from the plate, and cells were treated with 25  $\mu$ L solution of each compound at 10  $\mu$ M and incubated at 37 °C for 10 min followed by addition of 25  $\mu$ L of amyloid Beta (American peptide, 1–42) solution at 10  $\mu$ M. Cells were incubated at 37 °C for 7 h and washed twice with PBS. Cells were lysed by using 1% Triton-X 100 in TBST buffer solution and protein concentrations of each well were determined via BCA protein determination kit (Thermo scientific). Equal amount of cell lysates from each well were plated into a white 96-well plate (NUNC) and the amount of ATP levels in each sample was determined

by using ATP determination kit (Invitrogen). The ATP levels of each sample were subtracted with vehicle control and percent inhibition were calculated based on the ATP levels of the vehicle control treated with amyloid Beta. ATP-based cell viability was also calculated based on the ATP levels of each sample without the treatment of amyloid Beta solution.

#### **4.2.5. Assay of Protection against A $\beta$ -induced cytotoxicity**

5000 HT-22 cells per well were seeded and treated as above described method. Cells were incubated at 37 °C for 24 h. 10  $\mu$ L of MTT solution (Thiazolyl blue tetrazolium bromide, Sigma) was added directly to each well and incubated at 37 °C for 2 h. After confirming the formation of blue formazan precipitates under microscope, 140  $\mu$ L of solubilizing solution (10% Triton-X 100 in Isopropanol with 0.1 M HCl) was added to each well followed by incubation for another hour at room temperature. Absorbance at 570 nm was measured and OD values from each well were subtracted with vehicle control and percent inhibition and cell viability were calculated by using the same method described for the ATP assay.

#### **4.2.6. Assay of Protection against A $\beta$ -induced ROS production**

10,000 HT-22 cells per well were seeded in black/clear bottom plate and treated with each compound and amyloid Beta in Opti- MEM for 6 h. Cells were washed once with HBSS. 100  $\mu$ L of CMH<sub>2</sub>DCFDA (Invitrogen C6827) solution, prepared from dilution of 2  $\mu$ L of the 1mM stock solution into 2 mL media (HBSS), was added into each well. Cells were incubated at 37 °C for 30 min and washed twice with HBSS. 100  $\mu$ L of nuclear staining (Hoechst), prepared from dilution of 1  $\mu$ L of nuclear staining into 1 mL HBSS, were added into each well. ROS production was measured by capturing fluorescent images from each well, and then calculated the total

signal intensity from each well by using Operetta high content screening system (Perkin Elmer). Percent inhibition against A $\beta$ -induced ROS production was determined by calculating percent ratio of the increased total signal intensity from compounds treated cells to untreated cells in the presence of A $\beta_{1-42}$ .

#### **4.2.7. Parallel artificial membrane permeability assay (Assay of diffusion across BBB)**

The effective permeabilities of the tested compounds, as well as, three known drugs were determined using Double-Sink™ (Pion, BBB-PAMPA) employing a donor 96 well-plate microtitre and an acceptor 96-well filter plate to form a sandwich such that each well is divided into two chambers, separated by a BBB-PAMPA lipid membrane. DMSO stock solutions of tested compounds (10 mM) and reference drugs (10 mM) were prepared and diluted with Prisma buffer solution (pH = 7.4) to provide test solutions of 50 $\mu$ M concentration which was placed in the wells of the donor plate. The acceptor plate containing Brain Sink Buffer was placed to form a sandwich and allowed to incubate for 4hours at 26°C. The acceptor plate was removed and the concentration of compounds in the acceptor, the donor, and the reference wells were measured by UV (230-498 nm). The effective permeability,  $P_e$ , of each compound was calculated using Pion PAMPA Explorer software (version 3.8) applying calculation basis double sink (acceptor+donor+membrane). The following  $P_e$  ranges were established: no penetration of BBB ( $P_e < 0.4 \times 10^{-6}$ ), penetration of BBB ( $P_e > 0.4 \times 10^{-6}$ ), low CNS bioavailability ( $P_e < 10 \times 10^{-6}$ ), and high CNS bioavailability ( $P_e > 10 \times 10^{-6}$ ).

#### **4.2.8. Molecular docking**

The three-dimensional structure of human CypD in complex with CsA (pdb code: **2Z6W**) was retrieved from protein databank. Using protein preparation tool in Discovery Studio 4.0 (Accelrys, San Diego, CA, USA), the receptor was prepared for docking. Ligands were sketched in ChemBioDraw program and then prepared generating the minimized 3D structures using Ligand Preparation tool in Discovery Studio 4.0. Docking minimization was done using CDocker algorithm implemented in Discovery Studio 4.0. The calculated docked poses were subjected to *in situ* ligand minimization within the binding pocket with estimation of binding energy and complex energy. The results were visualized and analyzed using tools implemented in Discovery Studio 4.0.

#### **4.2.9. hERG K<sup>+</sup> channel assay**

[<sup>3</sup>H] Astemizole and human ERG K<sup>+</sup> channel expressed in HEK-293 cells were purchased from PerkinElmer. Assays were performed in 200 µL of 50 mM Hepes (pH 7.4), 60 mM KCl, 0.1% BSA, 4 nM [<sup>3</sup>H] Astemizole with 2.5 µg of membranes. Assay mixtures were incubated for 1h at room temperature (RT) and filtered through a Filtermat-A pre-soaked in 0.3% PEI. The signal was detected with a MicroBeta<sup>®</sup> (PerkinElmer). Non-specific binding was determined in the presence of 0.1 µM astemizole. Competition binding studies were carried out with 5–6 varied concentrations of the test compound run in duplicate tubes, and isotherms from two assays were calculated.

#### **Conflict of interest**

The authors have declared no conflict of interest.

## Acknowledgments

This work was supported by the KIST Institutional programs (Grant No. 2E26090) from Korea Institute of Science and Technology and by the Creative Fusion Research Program through the Creative Allied Project funded by the National Research Council of Science & Technology (CAP-12-1-KIST).

## References

- [1] H. Checkoway, J.I. Lundin, S.N. Kelada, Neurodegenerative diseases, IARC scientific publications, (2011) 407-419.
- [2] A. Abbott, Dementia: A problem for our age, *Nature*, 475 (2011) S2-S4.
- [3] E.R. Dorsey, B.P. George, B. Leff, A.W. Willis, The coming crisis: obtaining care for the growing burden of neurodegenerative conditions, *Neurology*, 80 (2013) 1989-1996.
- [4] A.s. Association, 2015 Alzheimer's Disease Facts and Figures, in, Alzheimer's Association, 2015.
- [5] M.S. Forman, J.Q. Trojanowski, V.M.Y. Lee, Neurodegenerative diseases: a decade of discoveries paves the way for therapeutic breakthroughs, *Nat Med*, 10 (2004) 1055-1063.
- [6] H. Chen, D.C. Chan, Mitochondrial dynamics—fusion, fission, movement, and mitophagy—in neurodegenerative diseases, *Human Molecular Genetics*, 18 (2009) R169-R176.
- [7] J.J. Palop, J. Chin, L. Mucke, A network dysfunction perspective on neurodegenerative diseases, *Nature*, 443 (2006) 768-773.
- [8] D.E. Bredesen, R.V. Rao, P. Mehlen, Cell death in the nervous system, *Nature*, 443 (2006) 796-802.
- [9] P.I. Moreira, X. Zhu, X. Wang, H.-g. Lee, A. Nunomura, R.B. Petersen, G. Perry, M.A. Smith, Mitochondria: A therapeutic target in neurodegeneration, *Biochimica et Biophysica Acta (BBA) - Molecular Basis of Disease*, 1802 (2010) 212-220.
- [10] B. Su, X. Wang, L. Zheng, G. Perry, M.A. Smith, X. Zhu, Abnormal mitochondrial dynamics and neurodegenerative diseases, *Biochimica et Biophysica Acta (BBA) - Molecular Basis of Disease*, 1802 (2010) 135-142.
- [11] P.I. Moreira, C. Carvalho, X. Zhu, M.A. Smith, G. Perry, Mitochondrial dysfunction is a trigger of Alzheimer's disease pathophysiology, *Biochimica et Biophysica Acta (BBA) - Molecular Basis of Disease*, 1802 (2010) 2-10.
- [12] K.F. Winklhofer, C. Haass, Mitochondrial dysfunction in Parkinson's disease, *Biochimica et Biophysica Acta (BBA) - Molecular Basis of Disease*, 1802 (2010) 29-44.
- [13] P. Shi, J. Gal, D.M. Kwinter, X. Liu, H. Zhu, Mitochondrial dysfunction in amyotrophic lateral sclerosis, *Biochimica et Biophysica Acta (BBA) - Molecular Basis of Disease*, 1802 (2010) 45-51.
- [14] M. Damiano, L. Galvan, N. Déglon, E. Brouillet, Mitochondria in Huntington's disease, *Biochimica et Biophysica Acta (BBA) - Molecular Basis of Disease*, 1802 (2010) 52-61.
- [15] E. Lezi, R.H. Swerdlow, Mitochondria in neurodegeneration, *Advances in experimental medicine and biology*, 942 (2012) 269-286.
- [16] M.T. Lin, M.F. Beal, Mitochondrial dysfunction and oxidative stress in neurodegenerative diseases, *Nature*, 443 (2006) 787-795.

- [17] J.-S. Kim, L. He, J.J. Lemasters, Mitochondrial permeability transition: a common pathway to necrosis and apoptosis, *Biochemical and Biophysical Research Communications*, 304 (2003) 463-470.
- [18] A. Rasola, P. Bernardi, The mitochondrial permeability transition pore and its involvement in cell death and in disease pathogenesis, *Apoptosis*, 12 (2007) 815-833.
- [19] A. Sessa, J.E. Belizario, M.M. Marques, M.L. Higuchi, R.I. Schumacher, A. Colquhoun, E. Ito, J. Kawakami, Mitochondrial swelling and incipient outer membrane rupture in preapoptotic and apoptotic cells, *Anatomical record (Hoboken, N.J. : 2007)*, 295 (2012) 1647-1659.
- [20] R.A.J. Smith, R.C. Hartley, H.M. Cochemé, M.P. Murphy, Mitochondrial pharmacology, *Trends in Pharmacological Sciences*, 33 (2012) 341-352.
- [21] M.J. Hansson, S. Morota, L. Chen, N. Matsuyama, Y. Suzuki, S. Nakajima, T. Tanoue, A. Omi, F. Shibasaki, M. Shimazu, Y. Ikeda, H. Uchino, E. Elmér, Cyclophilin D-Sensitive Mitochondrial Permeability Transition in Adult Human Brain and Liver Mitochondria, *Journal of Neurotrauma*, 28 (2011) 143-153.
- [22] C.P. Baines, R.A. Kaiser, N.H. Purcell, N.S. Blair, H. Osinska, M.A. Hambleton, E.W. Brunskill, M.R. Sayen, R.A. Gottlieb, G.W. Dorn, J. Robbins, J.D. Molkenin, Loss of cyclophilin D reveals a critical role for mitochondrial permeability transition in cell death, *Nature*, 434 (2005) 658-662.
- [23] H. Du, S.S. Yan, Mitochondrial permeability transition pore in Alzheimer's disease: cyclophilin D and amyloid beta, *Biochimica et Biophysica Acta*, 1802 (2010) 198-204.
- [24] V.K. Rao, E.A. Carlson, S.S. Yan, Mitochondrial permeability transition pore is a potential drug target for neurodegeneration, *Biochimica et Biophysica Acta (BBA) - Molecular Basis of Disease*, 1842 (2014) 1267-1272.
- [25] J. Warne, G. Pryce, J. Hill, X. Shi, F. Lennerås, F. Puentes, M. Kip, L. Hilditch, P. Walker, M.I. Simone, A.W.E. Chan, G.J. Towers, A. Coker, M.R. Duchon, G. Szabadkai, D. Baker, D.L. Selwood, Selective inhibition of the mitochondrial permeability transition pore protects against neuro-degeneration in experimental multiple sclerosis, *Journal of Biological Chemistry*, (2015).
- [26] H. Du, L. Guo, F. Fang, D. Chen, A. A Sosunov, G. M McKhann, Y. Yan, C. Wang, H. Zhang, J.D. Molkenin, F.J. Gunn-Moore, J.P. Vonsattel, O. Arancio, J.X. Chen, S.D. Yan, Cyclophilin D deficiency attenuates mitochondrial and neuronal perturbation and ameliorates learning and memory in Alzheimer's disease, *Nat Med*, 14 (2008) 1097-1105.
- [27] M. Hansson, G. Mattiasson, R. Månsson, J. Karlsson, M. Keep, P. Waldmeier, U. Rugg, J.-M. Dumont, K. Besseghir, E. Elmér, The Nonimmunosuppressive Cyclosporin Analogs NIM811 and UNIL025 Display Nanomolar Potencies on Permeability Transition in Brain-Derived Mitochondria, *J Bioenerg Biomembr*, 36 (2004) 407-413.
- [28] J. Fu, M. Tjandra, C. Becker, D. Bednarczyk, M. Capparelli, R. Elling, I. Hanna, R. Fujimoto, M. Furegati, S. Karur, T. Kasprzyk, M. Knapp, K. Leung, X. Li, P. Lu, W. Mergo, C. Miault, S. Ng, D. Parker, Y. Peng, S. Roggo, A. Rivkin, R.L. Simmons, M. Wang, B. Wiedmann, A.H. Weiss, L. Xiao, L. Xie, W. Xu, A. Yifru, S. Yang, B. Zhou, Z.K. Sweeney, Potent Nonimmunosuppressive Cyclophilin Inhibitors With Improved Pharmaceutical Properties and Decreased Transporter Inhibition, *Journal of Medicinal Chemistry*, 57 (2014) 8503-8516.
- [29] H.-x. Guo, F. Wang, K.-q. Yu, J. Chen, D.-l. Bai, K.-x. Chen, X. Shen, H.-l. Jiang, Novel cyclophilin D inhibitors derived from quinoxaline exhibit highly inhibitory activity against rat mitochondrial swelling and Ca<sup>2+</sup> uptake/release, *Acta Pharmacol Sin*, 26 (2005) 1201-1211.
- [30] S. Murasawa, K. Iuchi, S. Sato, T. Noguchi-Yachide, M. Sodeoka, T. Yokomatsu, K. Dodo, Y. Hashimoto, H. Aoyama, Small-molecular inhibitors of Ca<sup>2+</sup>-induced mitochondrial permeability transition (MPT) derived from muscle relaxant dantrolene, *Bioorganic & Medicinal Chemistry*, 20 (2012) 6384-6393.
- [31] Y.S. Kim, S.h. Jung, B.-G. Park, M.K. Ko, H.-S. Jang, K. Choi, J.-H. Baik, J. Lee, J.K. Lee, A.N. Pae, Y.S. Cho, S.-J. Min, Synthesis and evaluation of oxime derivatives as modulators for amyloid beta-induced mitochondrial dysfunction, *European Journal of Medicinal Chemistry*, 62 (2013) 71-83.

- [32] S.h. Jung, K. Choi, A.N. Pae, J.K. Lee, H. Choo, G. Keum, Y.S. Cho, S.-J. Min, Facile diverted synthesis of pyrrolidinyl triazoles using organotrifluoroborate: discovery of potential mPTP blockers, *Organic & Biomolecular Chemistry*, 12 (2014) 9674-9682.
- [33] S.G. Agalave, S.R. Maujan, V.S. Pore, Click chemistry: 1,2,3-triazoles as pharmacophores, *Chemistry, an Asian journal*, 6 (2011) 2696-2718.
- [34] B.K. Wagner, T. Kitami, T.J. Gilbert, D. Peck, A. Ramanathan, S.L. Schreiber, T.R. Golub, V.K. Mootha, Large-scale chemical dissection of mitochondrial function, *Nat Biotech*, 26 (2008) 343-351.
- [35] S.T. Smiley, M. Reers, C. Mottola-Hartshorn, M. Lin, A. Chen, T.W. Smith, G.D. Steele, L.B. Chen, Intracellular heterogeneity in mitochondrial membrane potentials revealed by a J-aggregate-forming lipophilic cation JC-1, *Proceedings of the National Academy of Sciences*, 88 (1991) 3671-3675.
- [36] S.P.M. Crouch, R. Kozlowski, K.J. Slater, J. Fletcher, The use of ATP bioluminescence as a measure of cell proliferation and cytotoxicity, *Journal of Immunological Methods*, 160 (1993) 81-88.
- [37] P. Carrillo-Mora, R. Luna, Col, #xed, L. n-Barenque, Amyloid Beta: Multiple Mechanisms of Toxicity and Only Some Protective Effects?, *Oxidative Medicine and Cellular Longevity*, 2014 (2014) 15.
- [38] W. Danysz, C.G. Parsons, Alzheimer's disease,  $\beta$ -amyloid, glutamate, NMDA receptors and memantine – searching for the connections, *British Journal of Pharmacology*, 167 (2012) 324-352.
- [39] T. Saito, T. Suemoto, N. Brouwers, K. Slegers, S. Funamoto, N. Mihira, Y. Matsuba, K. Yamada, P. Nilsson, J. Takano, M. Nishimura, N. Iwata, C. Van Broeckhoven, Y. Ihara, T.C. Saido, Potent amyloidogenicity and pathogenicity of A[ $\beta$ ]43, *Nat Neurosci*, 14 (2011) 1023-1032.
- [40] I. Benilova, B. De Strooper, An overlooked neurotoxic species in Alzheimer's disease, *Nat Neurosci*, 14 (2011) 949-950.
- [41] N. Izzo, A. Staniszewski, L. To, M. Fa, A. Teich, F. Saeed, H. Wostein, T. Walko, A. Vaswani, M. Wardius, Z. Syed, J. Ravenscroft, K. Mozzoni, C. Silky, C. Rehak, R. Yurko, P. Finn, G. Look, G. Rishton, H. Safferstein, M. Miller, C. Johanson, E. Stopa, M. Windisch, B. Hutter-Paier, M. Shamloo, O. Arancio, H. LeVine, S. Catalano, Alzheimer's therapeutics targeting amyloid beta 1-42 oligomers I: Abeta 42 oligomer binding to specific neuronal receptors is displaced by drug candidates that improve cognitive deficits, *PLoS one*, 9 (2014).
- [42] M.P. Mattson, Pathways towards and away from Alzheimer's disease, *Nature*, 430 (2004) 631-639.
- [43] M.V. Berridge, A.S. Tan, Characterization of the Cellular Reduction of 3-(4,5-dimethylthiazol-2-yl)-2,5-diphenyltetrazolium bromide (MTT): Subcellular Localization, Substrate Dependence, and Involvement of Mitochondrial Electron Transport in MTT Reduction, *Archives of Biochemistry and Biophysics*, 303 (1993) 474-482.
- [44] G. Ye, N.S. Metreveli, J. Ren, P.N. Epstein, Metallothionein prevents diabetes-induced deficits in cardiomyocytes by inhibiting reactive oxygen species production, *Diabetes*, 52 (2003) 777-783.
- [45] L. Di, E.H. Kerns, K. Fan, O.J. McConnell, G.T. Carter, High throughput artificial membrane permeability assay for blood-brain barrier, *European Journal of Medicinal Chemistry*, 38 (2003) 223-232.
- [46] J. RUELL, Membrane-based drug assays, *Modern Drug Discovery*, 6 (2003) 28-30.
- [47] K. Kajitani, M. Fujihashi, Y. Kobayashi, S. Shimizu, Y. Tsujimoto, K. Miki, Crystal structure of human cyclophilin D in complex with its inhibitor, cyclosporin A at 0.96-Å resolution, *Proteins*, 70 (2008) 1635-1639.
- [48] G. Wu, D.H. Robertson, C.L. Brooks, M. Vieth, Detailed analysis of grid-based molecular docking: A case study of CDOCKER—A CHARMM-based MD docking algorithm, *Journal of Computational Chemistry*, 24 (2003) 1549-1562.
- [49] C. Jamieson, E.M. Moir, Z. Rankovic, G. Wishart, Medicinal chemistry of hERG optimizations: Highlights and hang-ups, *J Med Chem*, 49 (2006) 5029-5046.
- [50] A.A. Lagrutta, E.S. Trepakova, J.J. Salata, The hERG channel and risk of drug-acquired cardiac arrhythmia: an overview, *Current topics in medicinal chemistry*, 8 (2008) 1102-1112.

[51] C.W. Murray, M.J. Hartshorn, M. Frederickson, M.S. Congreve, A. Padova, S.J. Woodhead, A.L. Gill, A.J. Woodhead, Preparation of 3-[heteroaryl-methoxy]pyridines and their analogues as p38 map kinase inhibitors, in, Astex Technology Limited, UK . 2004, pp. 134 pp.

[52] J.A. Bristol, I. Gross, R.G. Lovey, An improved synthesis of 2-amino-3-alkoxy-pyridines by a phase-transfer catalyzed ether synthesis, *Synthesis*, (1981) 971-973.

ACCEPTED MANUSCRIPT

## Highlights

- The inhibitory activity of seventeen compounds against A $\beta$ -induced mPTP opening was superior to that of the standard Cyclosporin A (CsA).
- Among all, 1-(3-(benzyloxy)pyridin-2-yl)-3-(2-(piperazin-1-yl)ethyl)urea (**5x**) effectively maintained mitochondrial function and cell viabilities on ATP assay, MTT assay, and ROS assay.
- Using CDocker algorithm, a molecular docking model presented a plausible binding mode for **5x** with cyclophilin D (CypD) receptor as a major component of mPTP.
- hERG assay presented a safe cardiotoxicity profile of **5x**.